An experimental investigation on the indoor hygrothermal environment of a reinforced-EPS based temporary housing solution

An experimental investigation on the indoor hygrothermal environment of a reinforced-EPS based temporary housing solution

M. D'Orazio[a], G. Maracchini[a]

[a] Department of Civil and Building Engineering and Architecture (DICEA), Polytechnic University of Marche, via Brecce Bianche, 60131, Ancona, Italy

E-mail addresses: m.dorazio@staff.univpm.it; g.maracchini@staff.univpm.it

ABSTRACT

In a post-disaster scenario, temporary lightweight housing solutions are generally used for quickly providing disaster victims with a temporary living place. Developed for limited periods of occupation and typically built shortly with lightweight technologies, people can end up living in these buildings, especially in low-income countries, for years or even decades. Considering a possible long-occupation period, it is necessary to improve the ability of these building to grant adequate comfort even considering their temporary character. Nevertheless, few studies in the literature are focused on the indoor thermal comfort environment of these buildings. This paper shows some results of a study addressed to analyze and improve the indoor hygrothermal behavior of a novel, modular and lightweight temporary housing solution, named HOMEDONE, based on the assembly of 3D-reinforced EPS panels. After a preliminary characterization of the system in terms of *in situ* thermal transmittance and airtightness performance, useful to provide a reference for the numerical simulations, the indoor hygrothermal behavior of an experimental unit is monitored during the spring and the summer season. Then, hygrothermal simulations are carried out to verify the occurrence of the experimentally observed moisture-related issues in different climatic contexts and to evaluate the effectiveness of possible improvement solutions. The results showed a low *in situ* thermal transmittance and good airtightness performance of the HOMEDONE construction system. However, the experimental measurements revealed that, at closed opening condition, indoor air temperature and relative humidity can be very high and unacceptable during the cooling season, due to the low thermal storage capacity and the low moisture buffering/water absorption capacity of the building components. The simulations demonstrate that an internal finishing layer with adequate moisture buffering capacity can significantly reduce RH levels, preventing condensation issues and mold growth. Nevertheless, the use of the HOMEDONE unit for long periods of occupation is discouraged, especially in hot climates, unless appropriate measures to reduce the indoor overheating and to improve thermal comfort are adopted.

KEYWORDS

Temporary housing; Affordable housing; Prefabricated house; Reinforced EPS; *In situ* thermal transmittance; Airtightness; Hygrothermal environment; Hygrothermal modeling; Mold growth; Moisture buffering.

1 INTRODUCTION

In recent years, dramatic events such as conflicts, natural disasters and migrant crisis are increasingly frequent due to climate change [1,2]. After these events, people tend to be shocked, traumatized and extremely worried about their future because of the losses of their relatives, friends, goods and belongings.

Housing provision has a crucial role in the recovery process, allowing people to re-establish some normalcy in their life, providing the conditions to live with protection, security, comfort and privacy, and also preventing the rising of deaths and the spread of diseases [3].

However, in a chaotic post-disaster situation providing new houses and repairing damaged ones may take time. Thus, in the meanwhile, it is mandatory to develop and provide temporary accommodations where locating people as quick as possible.

In an emergency scenario, two different types of temporary accommodations are generally provided: *temporary shelter*, which are mainly tents having the aim of quickly locating the maximum number of displaced people; *temporary housing*, i.e. more durable lightweight prefabricated accommodations that replace temporary shelters and provide people with the minimum conditions to live with dignity, privacy and protection, also allowing the resumption of everyday activities [3–7].

Temporary houses are generally modular and prefabricated construction systems designed for rapid construction and short periods of occupancy. As a result, the indoor hygrothermal environment is often treated as a secondary aspect in the design process, while airtightness performance is generally poor due to the presence of a large number of junctions that constitute potential air leakage paths, affecting thermal comfort, noise and fire resistance, and causing condensation problems [8–13].

Considering the different climatic conditions in which these buildings can be placed, and the possible lack in an emergency scenario of a suitable environment control system, unacceptable indoor hygrothermal environmental conditions often occur during the stay of displaced people, such as extremely high temperatures in summer and coldness in winter, which, as well known, may cause diseases and mortality to people after a prolonged exposure.

Despite this, it is not uncommon that forcibly displaced people end up living in these buildings for years or even

decades, turning emergency camps in semi-permanent settlements [14]. To date, in fact, it is estimated that over 60 million people all around the world live in temporary accommodations in the condition of displacement [15–17]. In this framework, investigating the indoor hygrothermal environment of these construction systems become mandatory, also to allow a correct improvement of their hygrothermal performance before or during their service life [5,18–20].

However, while the indoor hygrothermal environment of conventional permanent buildings has been widely investigated in literature [8–10], there are only a few recent studies focused on the indoor thermal environment of temporary lightweight units. For example, in [21], the indoor hygrothermal environment of a prefabricated house made of insulated color metal sheet sandwich panels was investigated. The authors found that the thermal conditions inside the unit, placed in the subtropics, is highly unacceptable for long term occupation, with the air temperature very high in summer at daytime (with closed door and windows) and no thermal shift. In [22], the indoor thermal environment and comfort condition of Nepalese self-made temporary shelters made of zinc or tarpaulin sheets was studied. They found that the adopted construction materials are marginally useful as insulation and for mitigating discomfort. In [23], the authors investigated the indoor hygrothermal environment of a building module prototype composed of wood and multilayer agglomerated cork panels. The experimental results showed a thermal shift of 3h and 45min. In [24], the characteristics of the indoor thermal environment of a novel temporary housing solution in Korea was studied in order to assess energy and comfort performance. The results showed that the thermal environment is not always comfortable for occupants in both summer and winter. A lower yearly energy demand than that related to existing temporary housing was also obtained. In [25], the indoor environmental conditions in two desert refugee camps in northern Jordan were investigated. They found that refugees were very unsatisfied with the thermal conditions in their shelters, especially in summer. In [26], field measurement of the indoor thermal environment of one-story low-cost and low-energy prefab buildings made of expandable polystyrene sandwich boards placed in a temporary settlement with high building density was investigated. The authors found that the indoor thermal environment of prefab houses in summer was worse than that in winter with very poor indoor ventilation and micro-scale heat island effect. In [27], the airtightness performance of four types of common container houses (CH) made of 6-8 cm insulated panels externally covered by wood sliding or corrugated metal sheets was investigated through the fan pressurization method. The authors found that typical container houses have poor airtightness performance due to the low quality of junction detailing, still suffering from heat loss and condensation phenomena. They conclude highlighting the need to enhance airtightness and thermal resistance of CH envelope with properly-sealed and insulated junction detailing, by adopting thermal breaks and airtight sealants at junctions with thicker thermal insulation infills.

Among low-cost prefabricated building technologies potentially suitable for temporary and affordable accommodations, those based on synthetically produced materials (such as EPS walls) present several advantages in terms of sustainability and affordability [28,29]. However, there are only a few studies in literature focused on the implementation of these materials for temporary or affordable housing solutions and on the study of their indoor hygrothermal behavior [28].

In this paper, the results of an experimental and numerical campaign aimed at investigating the indoor hygrothermal behavior of a modular and lightweight construction system based on the assembly of prefabricated structural reinforced-EPS panels are reported. The construction system, named HOMEDONE, has been recently used as re-locatable temporary housing in post-earthquake scenarios in Central Italy (Marche Region) and as an affordable housing solution in developing countries to solve the increasing affordable housing demand [30].

Firstly, a characterization of the system is carried out in terms of *in situ* thermal transmittance and airtightness performance of an experimental unit located in the hot-summer Mediterranean climate of Ancona, Italy, recently stricken by a near seismic event (Central Italy earthquakes, 2016). The results of indoor hygrothermal measurements are then presented. Finally, the possible occurrence of moisture-related issues, such as internal surface condensation and mold growth, is evaluated through hygrothermal simulations, also considering annual occupancy and different climatic scenarios. The possible reduction of these issues by increasing the moisture buffering capacity of the system (i.e. by adding internal finishing layers) is then numerically verified. A discussion on the obtained results is then reported, also through a comparison with other common temporary and permanent housing solutions.

2 PHASES, MATERIALS AND METHODS

2.1 Phases

The present study can be subdivided into five phases:

- in the first phase, the thermal characterization of the HOMEDONE reinforced-EPS panels is carried out by measuring the *in situ* thermal transmittance of an experimental unit, in order to complete available literature data and to provide a reference for future analytical and numerical simulations, which are essential to define the correct strategy for the improvement of the system hygrothermal/comfort performance;
- in the second phase, since a modular and dry construction system may suffer from air leakages [27], and since airtightness performance are essential for future energy and comfort numerical simulations, a characterization of the system in terms of airtightness is also carried out through the fan pressurization method ("*Blower Door*

Tests");

- in the third phase, the indoor hygrothermal behavior of the experimental unit is measured during the spring and summer seasons, while any possible internal condensation issue is identified;
- then, considering the issues observed during the third phase (very high indoor air RH due to internal surface condensation), hygrothermal dynamic simulations are carried out to verify and quantify the occurrence of moisture-related issues such as condensation and mold growth risk during annual occupancy, also extending the results to a wider range of climatic contexts;
- finally, hygrothermal simulations are carried out to demonstrate the possibility of preventing moisture-related issues through the addition of an internal layer with moisture buffering capacity in all the considered climatic scenarios.

2.2 The HOMEDONE construction system

The HOMEDONE construction system is based on the assembly of prefabricated structural panels made of reinforced-EPS (Fig. 1), consisting of a high strength tridimensional electro-welded galvanized steel wire (S235JR [31]) embedded in a high-density EPS panel (from 45 kg/m^3 to 65 kg/m^3). The embedded wire is made of steel bars with a diameter of 3 mm and can be provided in different form and dimensions depending on the requests. The resulting panels can have different lengths (generally 1.2m), widths (from 10 to 16 cm) and heights (from 2.4 to 3.4 m). Due to their limited size and weight, they are easy to be transported and handled without the help of cranes.

HOMEDONE housing units may be provided both as readymade units, i.e. totally manufactured in the factory and then transported to their future place, or as kit supplies, allowing a total assembly in the site optimizing and reducing transportation costs [3]. Thanks to a patented steel hooking system, the panels assembly is fast and intuitive, allowing a manually tying of panels by using a simple Allen wrench. This is an important feature since the construction system is designed to be suitable even for not urbanized areas, where work-site vehicles may not have easy access and specialized workers may not be not present. Silicone glue is used to ensure air and water impermeability in the junctions between panels. Finally, based on requests an internal and external finishing layer can be applied, generally made of plastic sheet, steel sheet or multi-layer finishing systems.

In order to reduce the polluting impact on the site where the unit is placed and to restore more easily its original condition as in pre-disaster, a set of steel beams with steel rods can be used as foundation and for horizontality regulation. Moreover, thanks to the modularity, high adaptability to any spatial requests, according to the different need and use, is ensured, also allowing progressive modification, expansions, upgrading, re-use and re-location from temporary sites to

permanent locations [5]. In fact, since temporary accommodations have often experienced problems with their future utilization, i.e. when they are no longer need, the module can be disassembled, sold, re-used for other purposes or even included in permanent construction [32] without any waste of resources [33].

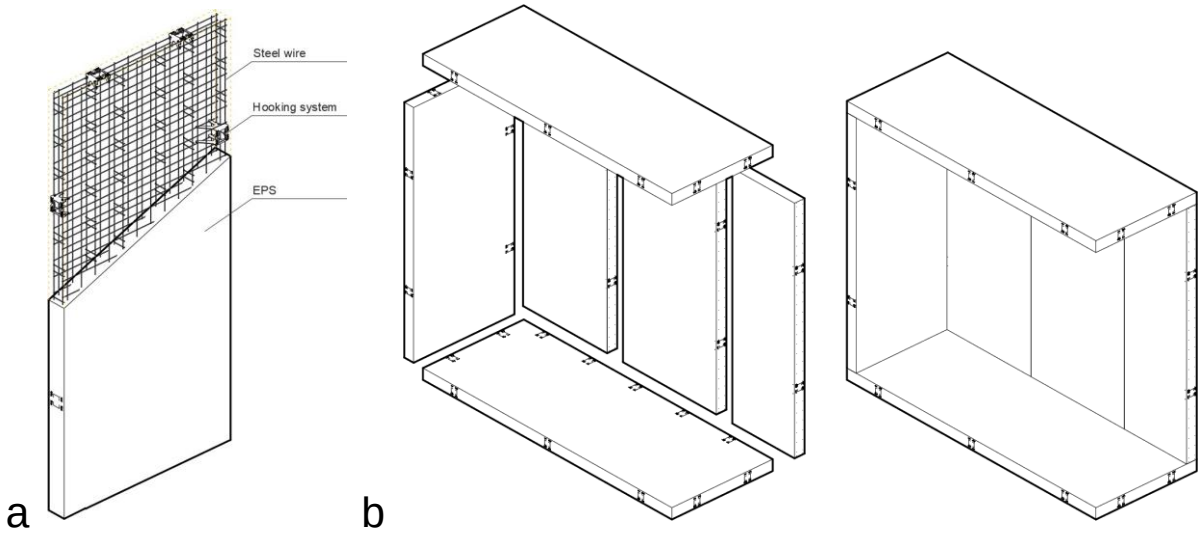

Fig. 1. a) Reinforced-EPS panel and b) assembly process of reinforced-EPS panels.

2.3 Description of the experimental housing unit

An experimental single-room unit with dimensions of 6.00 m (L) x 2.40 m (W) x 2.64 m (H) and a resulting floor area of 12.44 m^2 was exposed to the hot-summer Mediterranean climate of Ancona (Italy) [34] (Fig. 2). The unit represents the smallest available unit that can be used in an emergency situation (or for seasonal working purposes) and to realize multi-unit houses with more rooms. In Fig. 3, the geometrical characteristics of the experimental unit are reported. In particular, the unit was built off-site by using 24 reinforced-EPS panels with geometrical dimensions of 1.2 m (L) x 2.4 m (H) x 0.12 (W) m, excepting for the first and latter panels of the two longitudinal facades that have a length equal to 1.08 m. A single window and a single door were installed in the unit, both placed in the south side in order to simulate the worst condition in terms of solar exposure during hot season and ventilation that can occur in high-density settlements [26]. According to technical sheets, the double clear glazing window is characterized by a total solar transmission equal to 0.4, a light transmission equal to 0.630 and a *U-value* equal to 1.420 $Wm^{-2}K^{-1}$. The external door, a 24 mm thick glass fiber slab sandwiched between two thin layers of PVC, is instead characterized by a *U-value* of 1.305 $Wm^{-2}K^{-1}$.

In order to simulate the worst conditions even in terms of possible use, no finishing materials were applied and no electrical, architectural, water and air systems components were present. Air and water permeability were limited only by

sealing junctions and steel connections between panels with silicone sealant.

The construction phase took 4 hours. Then, the unit was placed on two external steel beams used as support and provided with external studs allowing horizontality regulation. As a result, the unit was not in direct contact with the soil but about 30 cm above the external ground.

a  b 

Fig. 2 a) Location of the experimental prefabricated unit inside the laboratory campus of the Polytechnic University of Marche and b) placing of the off-site assembled unit with the help of a crane.

169

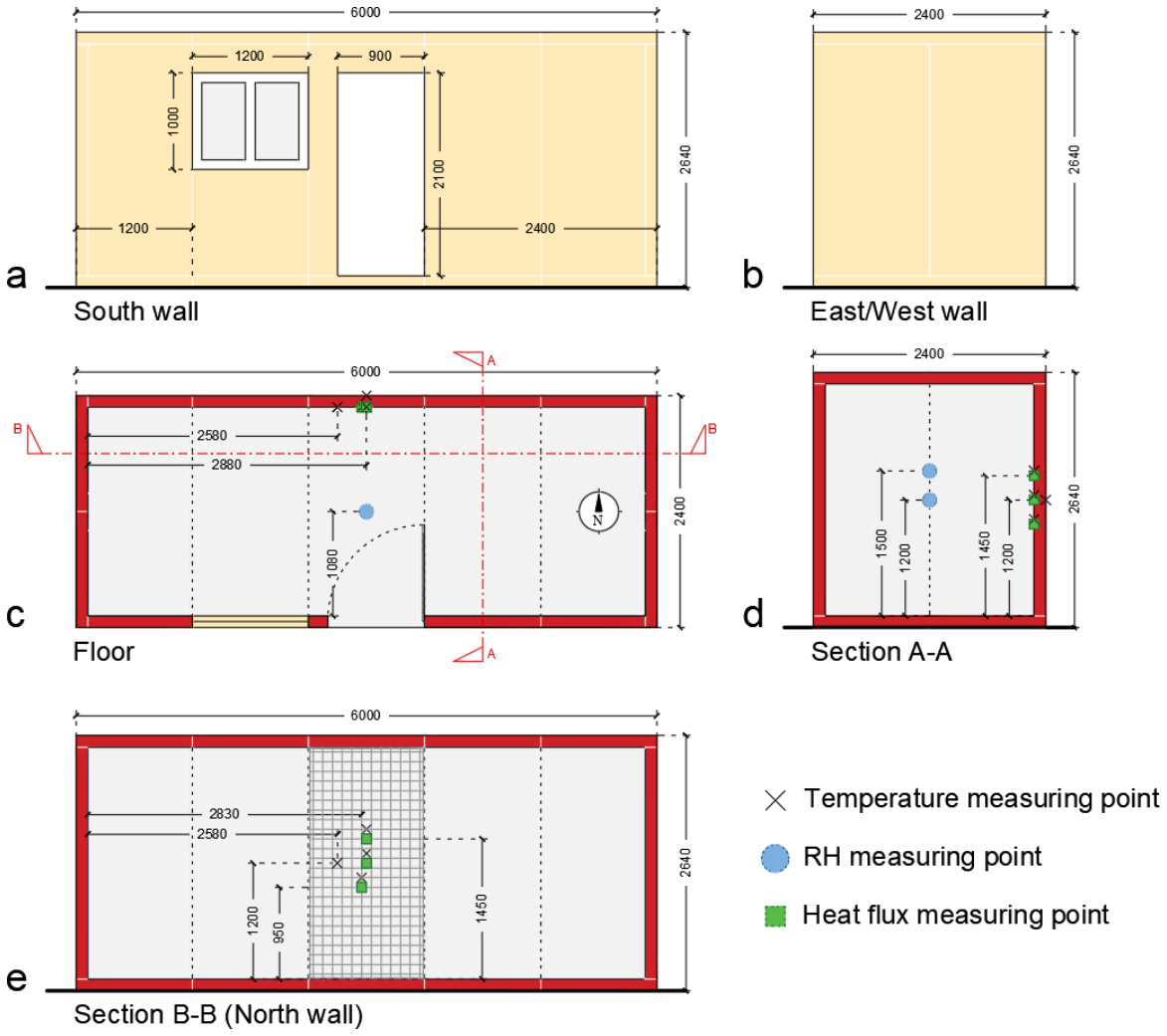
a
South wall
6000
1200
900
1000
2100
2640
1200
2400
b
East/West wall
2400
2640
c
Floor
6000
A
B
2580
2880
2400
1080
N
d
Section A-A
2400
1500
1200
1450
1200
2640
e
Section B-B (North wall)
6000
2830
2580
1200
950
1450
2640
Temperature measuring point
RH measuring point
Heat flux measuring point

170

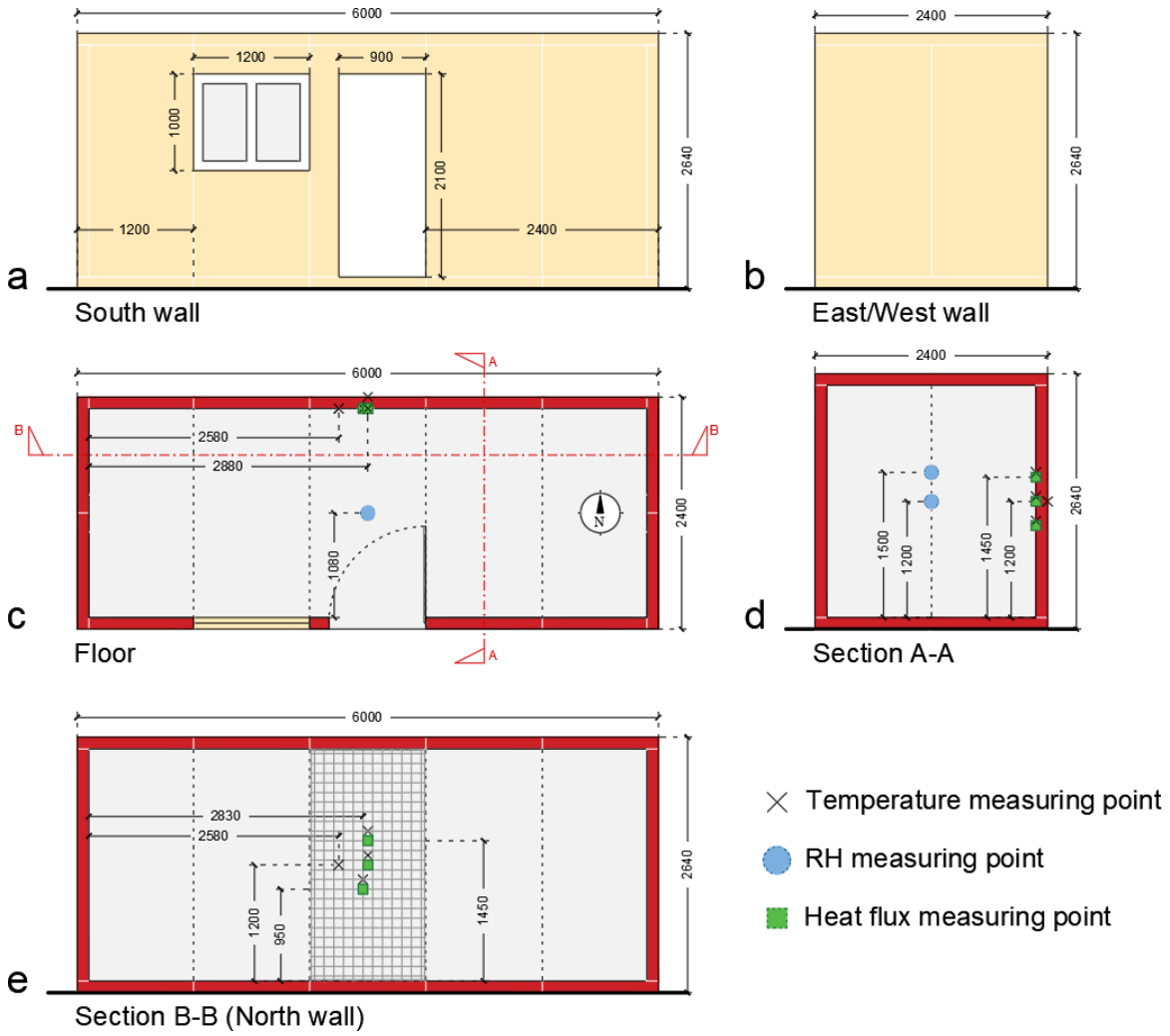

171

172 Fig. 3. Geometrical characteristics of the unit and temperature, Relative Humidity (RH) and heat flux measuring points inside and
173 outside the experimental unit. Dimensions in millimeters.

174 2.4 In situ thermal transmittance

175 The thermal transmittance (U-value) of a building component is the measure of the rate of heat transfer passing through
176 the element. In this work, the thermal transmittance of a reinforced-EPS panel was evaluated in order to complete available
177 literature data and to provide reliable transmittance values to be used in future analytical and numerical evaluations. Since
178 experimental transmittance values are generally considered more reliable than theoretical ones, especially in
179 multicomponent panels, the *in situ* thermal transmittance was computed in this study [35–39].

180 In particular, the *in situ* air-to-air and surface-to-surface U-values of the HOMEDONE panel (in the following called
181 transmittance U and conductance Λ, respectively) were measured through the heat flow meter method by following the
182 International Standard ISO 9869-1 [40].

The method consists of monitoring the heat flux rate passing through a façade and the indoor and outdoor surface/air temperatures. Since the accuracy of the results depends on the measuring conditions [41–43], according to ISO 9869-1 [40] the following measures were undertaken to provide reliability to the results:

- solar radiation on the tested sites was avoided by choosing the North-facing wall for all of the measurements;
- the thermocouple used to measure the external surface temperature, measured at the center of the middle panel of the North-facing façade, was accurately covered with white-colored duct tape in order to minimize the influence of external weather conditions such as rain, snow and direct solar radiation on measurements. The color of the tape was chosen in order to have an emissivity similar to the substrate (white EPS);
- the temperature and heat flux sensors were installed in a homogeneous location avoiding thermal bridges.

Concerning this latter point, homogeneity of the location on which surface sensors were installed was verified by placing three different heat flux thermal sensors and four thermocouples in different points on the middle panel of the North-facing walls. The different positions of the sensors, chosen in order to study the possible influence of the embedded steel bars on the surface temperatures, are reported in Fig. 3e, even in relation to the embedded steel wire mesh.

In particular, three Hukseflux Thermal Sensors HFP01 with a thermal resistance less than $6.25 \cdot 10^{-3}$ m^2K/W (considered negligible in relation to the total thermal resistance of the examined wall), a sensitivity of approximately 50 $\mu V m^2/W$ and an expected accuracy lying within ±5 % of the measured value were placed on the internal side of the north wall. PT-100 thermocouples (LSI Lastem) with an uncertainty of 0.1 °C at 0 °C were indeed used to measure internal and external surface temperatures. The indoor PT-100 were placed near to the heat flux meters, according to ISO 9869-1 [40]. To ensure good thermal contact between sensors and EPS surfaces, a layer of thermal interface material was also applied.

Indoor and outdoor air temperatures were measured by means of two thermohygrometers DMA 572.1 LSI Lastem with an uncertainty of 0.1 °C at 0 °C and 1.5% RH. The indoor thermohygrometer was placed at the center of the module, at 1.2 m above the floor while the outdoor one was accurately shielded from rain, wind and solar radiations.

A data logger (LSI Lastem ELO105) sampled data every minute and stored the 10-min average data in its memory.

According to ISO 9869-1 [40], different methods can be used for calculating U-values from experimental data. In this study, the average method is adopted due to its simplicity in use and rapidity in exporting results compared to other methods [42]. Accordingly, transmittance U and conductance Λ can be computed as follow:

$$UU = \frac{\sum_{jj=1}^{nn} qq_{jj}}{\sum_{jj=1}^{nn} \left(TT_{iijj} - TT_{oojj} \right)} \quad (1)$$

$$\Lambda\Lambda = \frac{\sum_{jj=1}^{nn} qq_{jj}}{\sum_{jj=1}^{nn} \left(TT_{ssiijj} - TT_{ssoojj} \right)} \quad (2)$$

where q is the density of the heat flow rate per unit area (W/m^2), T_i and T_o are the indoor and outdoor air temperatures, respectively, and T_{si} and T_{so} are the indoor and outdoor surface temperatures, respectively. The measuring period depends on measuring conditions, type of the tested wall and U-value calculation method. The period of the measurements according to this calculation method is at least three days and ends when the results after three subsequent nights do not differ by more than 5% [40]. Since the construction is composed by light elements (i.e. with a specific heat capacity per unit area of less than 20 kJ/m^2 K), only night data were considered in the calculation, in order to avoid the effects of solar radiation on the results, as recommended in EN ISO 9869-1 [40].

Finally, since a high temperature difference between the indoor and outdoor environment is needed to provide U-values with low variability (3 °C at least according to [42]), only during this test an electrical heat-generation apparatus was introduced inside the unit in order to maintain a constant air temperature of about 24.5 °C ± 1.5 °C, ensuring a difference between indoor and outdoor temperature ranging between 5 °C and 11 °C depending on the outdoor temperature.

2.5 Airtightness

Modular and dry-assembled construction systems may suffer from air leakages [27]. For this reason, in this study, the airtightness performance of the studied modular construction system was investigated, also in order to allow a correct improvement of its thermal performance before or during its service life. In particular, the airtightness of the reinforced-EPS housing unit (Fig. 3) was computed by using the fan (de)pressurization method, also known as Blower Door Test (BDT), in accordance with ISO 9972 [44]. BDT is the most widely applied method for airtightness measurements both in literature and professional practice [45], and it is based on the mass conservation theory according to which the air flow passing through the fan is compensated by an equal amount of flow passing through the leakage of the envelope.

As already said, the tested unit, showed in Fig. 2 and Fig. 3, was provided without finishing layers in order to simulate the worst scenario in terms of airtightness. Junctions between panels were sealed by means of silicone sealant and no components related to electrical, architectural, water and air systems were present. The aim was to provide only a first insight into the airtightness performance of the construction system in the worst condition of use for the occupants.

In order to perform the test, a system capable of moving air into the indoor environment at the required airflow level is needed to obtain pressurization or depressurization of the indoor space. With this aim, an Infiltec Blower Door E-3 220v was connected to the door opening to depressurize/pressurize the indoor space (Fig. 4). Simultaneously, a digital

pressure and flow gauge (Infiltec DM4) with a pressure range of ±1250 Pa (accuracy of 0.1 Pa) and a flow range 50-11050 m^3/h (accuracy ±5%), was used to record pressure differences and airflow rates.

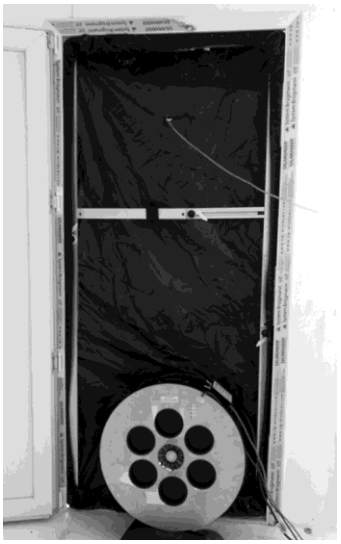

Fig. 4. Blower door test apparatus connected to the door opening of the unit.

Air flow measurements were performed considering four preparation methods of the unit:

- *Configuration 1: Building in use and building envelope*, in which normal use of the construction system was simulated with door and window simply closed;
- *Configuration 2: Sealed window*, in which in order to exclude air leakage paths (ALP) due to the window presence the joints between window and panels and the joints of the window were sealed;
- *Configuration 3: Sealed door*, in which the door was sealed against the wall panels. In this way, the ALP in the wall-door junctions were eliminated;
- *Configuration 4: Sealed openings*, in which both door and windows junctions were sealed. In this way, the air leakage of the construction system (i.e. without ALP due to opening insertion) was evaluated.

A comparison between the adopted configurations and those described in EN ISO 9972 [44] is reported in Table 1. In particular, configuration 1 is coherent with both Method 1 and Method 2 while the other three configurations are coherent with Method 3. From the comparison between the different results, the reduction in the building airtightness due to opening presence can be evaluated [9].

Table 1 Comparison between configurations of the unit suggested in EN ISO 9972 [44] and those used in this study for airtightness measurements.

Opening classification	EN ISO 9972 [44]			Methods in use			
	Method 1	Method 2	Method 3	Configuration 1	Configuration 2	Configuration 3	Configuration 4
	Building in use	Building envelope	Specific purpose	Building in use and envelope	Sealed window	Sealed door	Sealed openings
Ventilation opening for natural ventilation	closed	sealed	As specified	No such openings	No such openings	No such openings	No such openings
Openings for whole building mechanical ventilation or air conditioning	sealed	sealed	As specified	No such openings	No such openings	No such openings	No such openings
Opening for mechanical ventilation or air conditioning (only intermittent use)	closed	sealed	As specified	No such openings	No such openings	No such openings	No such openings
Windows	closed	closed	As specified	closed	sealed	closed	sealed
Doors and trapdoors in the envelope	closed	closed	As specified	closed	closed	sealed	sealed
Opening not intended for ventilation	closed	sealed	As specified	No such openings	No such openings	No such openings	No such openings

Before each test, the window was systematically opened for about 30 min. For each configuration, air flow values were measured for at least 5 pressure differences (Δp), set to be changed with 5 Pa intervals from the minimum pressure difference. This latter cannot be established a priori but it is defined as the pressure difference Δp that reaches the minimum airflow level recorded according to the sensitivity of the BDT apparatus (i.e. 50 m^3/h).

Corrections to the collected data for zero-flows pressure differences and internal/external air density differences were applied according to EN ISO 9972 [44]. For each configuration, the converted air flow rates for depressurization were then plotted on a log-log plot against the corresponding pressure differences. From the converted data, air flow coefficient C_{env} ($m^3/(h\ Pa^n)$) and air flow exponent n were determined by using the least-squares technique and equation (3):

$$qq_{eennee} = CC_{eennee} \cdot \Delta PP^{nn} \quad (3)$$

with q_{env} the air flow rate through the building envelope (m^3/h) and ΔP the induced pressure difference (Pa). Air flow coefficient C_{env} was then converted in C_L according to EN ISO 9972 [44] in order to represent ambient standard conditions (i.e. 20 °C and 101325 Pa). Then, the air leakage rate q_{pr} (m^3/h) at the reference pressure ΔP_r (Pa) can be calculated by equation (4):

$$qq_{pppp} = CC_{LL} \cdot \underset{pp}{\Delta PP}^{nn} \quad (4)$$

Through equation (4), it is possible to calculate the air leakage at the pressure reference (50 Pa), i.e. q_{50}. From this

value, the air change rate at 50Pa (n_{50}), the specific leakage rate (envelope) q_E and the specific leakage rate (floor) q_F can be calculated according to the following equations:

$$nn_{50} = \frac{qq_{50}}{VV} \quad (5)$$

$$qq_{EE} = \frac{qq_{50}}{AA_{EE}} \quad (6)$$

$$qq_{FF} = \frac{qq_{50}}{AA_{FF}} \quad (7)$$

where VV, AA_{EE} and AA_{FF} are the internal volume, the envelope area and the floor area of the depressurized space, respectively [44].

Finally, it should be noted that trial tests before and after testing were performed in order to find optimal testing conditions that, according to [44], include the following:

- the product of indoor-outdoor temperature difference and height of the building must be lower than 250 m K;
- wind speed near the ground or wind force in the Beaufort scale must be lower than 3.0 m/s or 3, respectively;
- the correlation coefficients obtained after testing for determining the air flow coefficient *C* and the air flow exponent *n* through the least-squares technique must be greater than 0.98;
- the air flow exponents *n* must range between 0.5 and 1.0.

The wind speed near the ground was visually quantified through the Beaufort scale and then checked by the wind velocity obtained by the near meteorological station. This latter was located at a higher level than the unit. Then, taking in mind that wind velocity usually rises with the increase of the height, if the wind speed of the meteorological station is smaller than the required wind speed near the ground, test results will surely meet the requirements [45,46].

2.6 Hygrothermal behavior

In order to investigate the indoor hygrothermal behavior of the HOMEDONE experimental unit, and then to allow the design of proper interventions for the improvement of its thermal comfort, indoor temperatures and RH of the experimental unit described in Section 2.3 and subject to the Mediterranean climate of Ancona, was measured for four months, i.e. from the 3 March 2017 to the 4 July 2017. In particular, the same instrumentation described in Section 2.4 was used for monitoring indoor and outdoor environment (air temperature and RH), indoor/outdoor surface temperatures and heat flux of the north wall (see Fig. 3). In addition, local weather parameters such as horizontal global solar radiation, horizontal diffuse radiation and atmospheric pressure were also monitored by using a near meteorological station.

During measurements, neither occupants nor HVAC systems were present inside the unit. Concerning the latter, it is

in fact not unusual that temporary houses are situated in remote areas without electricity. As a result, the indoor environment was only affected by environmental changes such as outdoor air temperature, solar radiation, etc. Concerning natural ventilation, in order to assemble the worst scenario, the window was initially closed, simulating a high-density emergency camp condition in which the air flow is blocked by other units. Then, a small opening of about 0.08 m^2 was introduced in order to simulate a scenario with a minimum of natural ventilation due to stack effect (which is added to the natural airflow through air leakage paths). The opening area was calculated in an approximated way based on averaged indoor-outdoor temperature differences so as to guarantee an average air change rate per hour of about 0.4 h^{-1} (without considering the presence of air leakage paths) according to [47,48].

Finally, some preliminary considerations on thermal comfort are made by computing the indoor thermal comfort for some representative days based on the adaptive thermal comfort model proposed in EN 15251 [47]. The latter is a widely used standard for building without cooling systems, recently adopted even for temporary ones (see e.g. [49]). Accordingly, the ranges of acceptable operative indoor temperatures T_c was obtained for each cooling day by using Eq. (8), where an acceptable limits equal to 80% corresponding to a normal level of expectation (category II) was assumed and some modifications to the original EN 15251 relationship were made in order to include all days of occupants' presence (i.e. those days with a weighted mean temperature of previous days T_{rm} lower than 10°C and higher than 30 °C [49]).

$$TT_{cc}=\begin{cases}(23.75\pm 3)\ ℃℃ & 𝕋_{pprr}<10℃℃\\ (20.75)℃℃\div(0.33𝕋_{pprr}+21.8)℃℃ & 10℃℃<𝕋_{pprr}<15℃℃\\ (0.33𝕋_{pprr}+18.8\pm 3)℃℃ & 15℃℃<𝕋_{pprr}<30℃℃\\ (28.70\pm 3)\ ℃℃ & 𝕋_{pprr}>30℃℃\end{cases} \quad (8)$$

The room operative temperature to be compared with T_c limits is assumed, in this work, as equal to the indoor air temperature T_i. This assumption, the accuracy of which is confirmed by preliminary numerical simulations, can be considered accurate enough for the aim of this work in which only a preliminary evaluation of thermal comfort is made. In particular, this assumption can be justified by: (i) the low percentage of window area of the unit that results in a small impact of the solar radiation on the mean radiant temperature; (ii) the small size and the null thermal storage capacity of the unit, which results in a negligible spatial variability of indoor air and surface temperatures [50]. However, further analyses will be carried out in future numerical and experimental works to deepen this aspect.

2.7 Condensation risk and moisture safety

In modular and dry construction systems, panel junctions constitute potential thermal bridges where moisture-related issues such as condensation and mold growth may occur. This may represent a risk for the occupants' health, especially when combined with unsuitable ventilation strategy [27,51,52]. For this reason, in our work, bidimensional dynamic

hygrothermal simulations were carried out to verify numerically the occurrence of moisture-related issues during the measuring period, and to extend the analysis to annual occupancy and different climatic scenarios.

The DELPHIN 6.0 hygrothermal software, developed at the Technical University of Dresden and successfully validated [53,54], was used at this aim, allowing simulating the coupled heat, moisture and matter transport in porous building materials by considering standard and natural climatic boundary conditions, such as temperature, RH, driving rain, wind speed, wind direction and short- and long-wave radiations [55]. The bidimensional hygrothermal model Fig. 5 was adopted to represent schematically the point at the roof and the wall junctions where higher heat flux is expected, i.e. at the steel connections (see Fig. 1).

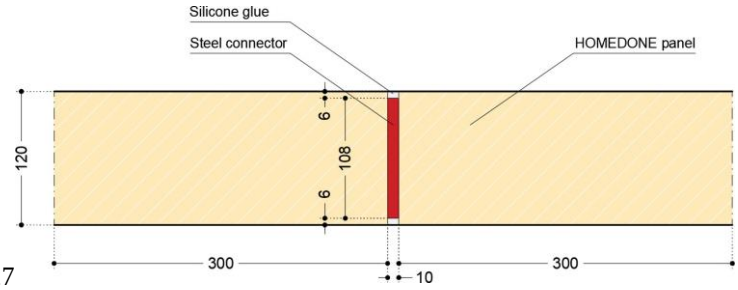

Fig. 5. Bidimensional schematic model of the HOMEDONE panels connection system at roof and wall junctions adopted for the hygrothermal simulations with the DELPHIN software [53]. A 0.1mm thick layer of air is used to measure with good approximation the internal surface RH of the vapor tight silicone glue. Dimension in millimeters.

The most relevant materials properties adopted in the calculation are reported in Table 2, mainly derived from the DELPHIN database [56]. Concerning EPS, the thermal conductivity of insulation materials may show a high dependency on temperature and RH/moisture content [57,58]. In high-density EPS, a quite small proportional increase of λ due to temperature variations is generally found (about 6 10^{-5} W/mK for a unitary increase of temperature [59,60]), along with an even smaller λ variation due to the moisture content (or RH) variability that may occur in EPS when subject to typical residential environments [61–64]. However, it is important to verify the impact of the temperature-dependency assumption on numerical results to verify the correctness of the constant λ hypothesis made in most energy simulation software [65]. For this reason, in our work, the resulting heat fluxes by assuming a temperature-dependent λ were compared with those obtained by assuming a constant λ [58]. According to the experimental λ-T relationships obtained for EPS materials with different densities in [59,60], a linear temperature-dependent function was adopted, characterized by a gradient of 6 10^{-5} W/mK according to [59,60] and passing through the experimental λ-T point obtained through the *in situ* measurements (see Section 2.4). The effect of RH was not considered due to its lower impact on λ values [57,63].

Table 2. Main hygric and thermal properties of the material adopted in DELPHIN 6.

Materials	EPS	Steel	Silicone glue*
Density [kg/m^3]	45	7800	3500
Thermal conductivity λ [W/(m K)]	Temperature-dependent function obtained from experimental results and literature [59]	47.0	3.3
Thermal capacity [J/kg K]	1500	470	1000
Vapor resistance coefficient [-]	50	200000	-
Hygroscopic sorption value at RH=80% [m^3/m^3]	6 10^{-4}	1.5 10^{-8}	-
Effective saturation (long-term process) [m^3/m^3]	0.935	1.5 10^{-6}	-
Water absorption coefficient [kg/(m^2 s$^{0.5}$)]	10^{-5}	10^{-6}	-

* Vapor tight

Concerning the outdoor boundary conditions, both extremely hot and extremely cold climates, also characterized by very different RH values, were considered in this study. In particular, in addition to the hot-summer Mediterranean climate of Ancona (Italy), the hot desert climate of Cairo (Egypt) and the humid continental climate of Oslo (Norway) were adopted. The main characteristics of the climatic data are reported in Table 3. This choice allows, on the one hand, extending the results to a wider range of climatic context. On the other hand, it allows finding solutions able to prevent moisture-related issues in almost any climatic context (i.e. including extreme climates), hence potentially allowing the use of the construction system at any latitude.

Concerning the indoor boundary conditions, for all the climatic contexts, the indoor air temperature and relative humidity were computed according to EN 15026 [66], considering a high occupancy of the building [56]. Initial moisture content and temperature of the building materials was set to 80% and 20°C, respectively, while the RH value corresponding to the condensation risk was set to 95%. A simulation period of four years was considered to reach a construction state in which the long-term water content does not change from year to year.

Table 3. Climates characteristics adopted in the hygrothermal simulations.

Location	Ancona, Italy	Oslo, Norway	Cairo, Egypt
Weather File	ASHRAE/IGDG, WMO 161910	ASHRAE/IWEC, WMO 014880	ASHRAE/IWEC, WMO 623660
Latitude [deg]	N 43.62	N 59.9	N 30.13
Longitude [deg]	E 13.52	E 10.62	E 31.40
Elevation [m]	105	17	74
Cooling degree days (base 25°C)	6	0	407
Cooling degree days (base 10°C)	1750	724	4277
Heating degree days (base 18°C)	2062	4162	389
Highest average monthly temperature [°C]	22.0	17.5	28.2
Highest average daily temperature [°C]	27.3	22.4	35.2
Lowest average monthly temperature [°C]	5.5	-3.8	14.0
Lowest average daily temperature [°C]	0.0	-13.2	11.4
Annual average solar global horizontal irradiance (GHI) [kWh m^{-2} day^{-1}]	3.25	2.41	5.26
Köppen classification	Csa (hot-summer mediterranean climate)	Dfb (humid continental climate)	BWh (hot desert climate)

Finally, the hygrothermal simulation results were used to estimate the mold growth risk on the junction internal surface. At this aim, the dynamic VTT model was adopted, allowing to take into account the RH and the temperature conditions, along with the sensitivity of the material to mold growth (material type and surface quality) [51]. According to this model, a mold growth index (*M*) ranging between 0 and 6 can be computed for each climate, representing the amount of mold mycelium growth on the material surface (see Table 4). According to the Ojanen's classification of material [67], the measurement point at the junction was modeled as medium resistant to mold growth, while assumptions on the safe side were made for the surface factor (very sensitive) and declination factor (sets to 0.1) [67,68].

Table 4. Mold index levels according to [67].

Mold index (*M*)	Description
0	No growth
1	Small amounts of mold on the surface (microscope) and initial stage of local growth
2	Several localized mold growth colonies on the surface (microscope)
3	Visual findings of mold on the surface (<10% coverage) or <50% coverage of mold (microscope)
4	Visual findings of mold on the surface (10-50% coverage) or >50% coverage of mold (microscope)
5	Plenty of growth on the surface, >50% visual coverage
6	Heavy and tight growth, coverage about 100%

2.8 Moisture buffering

Moisture buffering (MB) is the ability of the material surface to moderate the indoor humidity variations through adsorption and desorption. Since material with MB capacity can be used to control passively the indoor moisture condition and to reduce moisture-related issues, in this work hygrothermal simulations were carried out according to Section 2.7 to demonstrate the ability of MB layers in preventing condensation issues and mold growth.

In particular, two different internal MB layers were considered, i.e. a 3mm thick internal layer of cementitious finishing render (basecoat) and a 12.5mm thick gypsum plasterboard (directly fixed on the EPS panel). The materials properties of the MB layers are reported in Table 2, directly derived from the DELPHIN 6.0 database.

Concerning the VTT model, since the alkaline condition of new cementitious surfaces prohibits mold formation [68], the first year was excluded from the *M* calculation for the cementitious finishing layer.

Table 5. Main hygric and thermal properties of the material adopted in hygrothermal simulations.

Materials	Basecoat	Plasterboard
Density [kg/m^3]	1089	1133
Thermal conductivity [W/(m K)]	0.283	0.341
Thermal capacity [J/kg K]	1283	1228
Vapor resistance coefficient [-]	11.7	16.8
Hygroscopic sorption value at RH=80% [m^3/m^3]	0.092	0.019

Effective saturation (long-term process) [m^3/m^3]	0.301	0.526

Water absorption coefficient [kg/(m^2 s$^{0.5}$)]	0.059	0.057

3 RESULTS

3.1 In situ thermal transmittance

Before tests, the homogeneity of the measuring point location was checked by comparing temperature and heat flux values measured by sensors placed on the internal surface of the panel but in different locations (see Fig. 3e). As a result, no significant deviations between measured surface temperatures and heat flux measurements were noticed. Then, the embedded steel wire mesh did not affect significantly the homogeneity of the panel surface temperatures that, in turn, may be considered as homogeneous with a good approximation. Despite this, in the following the results obtained by averaging the measured indoor surface temperatures and heat fluxes were reported so as to obtain a representative average, according to ISO 9869-1 [31].

Fig. 6a reports the indoor and outdoor surface temperature values (T_{si} and T_{so}, respectively) and the heat flux q measured between 13 and 19 May 2017. In the same graph, the calculation of the conductance Λ (*in situ* surface-to-surface U-value) is also plotted. The obtained Λ is equal to 0.24 W/(m^2 K) from which the conductivity λ of the homogenized materials has been computed, i.e. λ=0.0288 W/(m K). Similarly, Fig. 6b reports the heat flux q with the indoor and outdoor air temperature values (T_i and T_o, respectively) measured between 13 and 19 May 2017. In the same graph, the calculation of the thermal transmittance U (*in situ* air-to-air U-value) is also reported. The obtained transmittance U is equal to 0.24 W/(m^2 K). The average temperature at mid-thickness of the EPS panel during the U-values calculation (useful to compute the temperature-dependent function of the EPS thermal conductivity λ in Section 3.4) was 20.1 °C.

In order to determine the influence of the steel wire mesh on the thermal properties of the panel, a comparison between the experimental values obtained in this work and the theoretical values calculated according to EN 13163 [69] for a simple EPS panels with same density (i.e. 45 kg/m^3) is carried out. In particular, the theoretical conductivity value is equal to λ=0.0315 W/(mK), i.e. slightly higher than the experimental value of the reinforced-EPS λ=0.0288 W/mK. Concerning the transmittance U, the theoretical one, computed by considering the theoretical conductivity λ=0.0315 W/(mK) and the surface resistances defined in EN ISO 6946 [70], is equal to 0.25 W/(m^2 K), which is higher than the experimental value U=0.24 W/(m^2 K). In both cases, a percentage difference of about 8-9% between theoretical and experimental values is found. Then, the embedded steel wire mesh seems not to affect the thermal properties of the EPS panel.

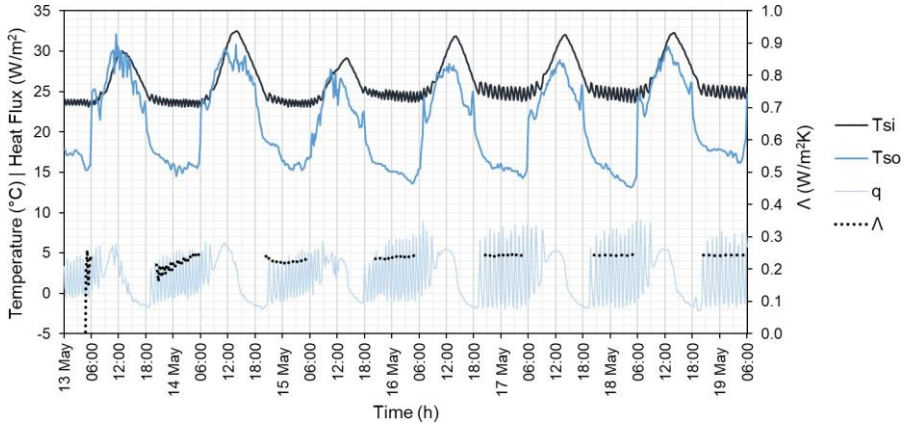

405 a

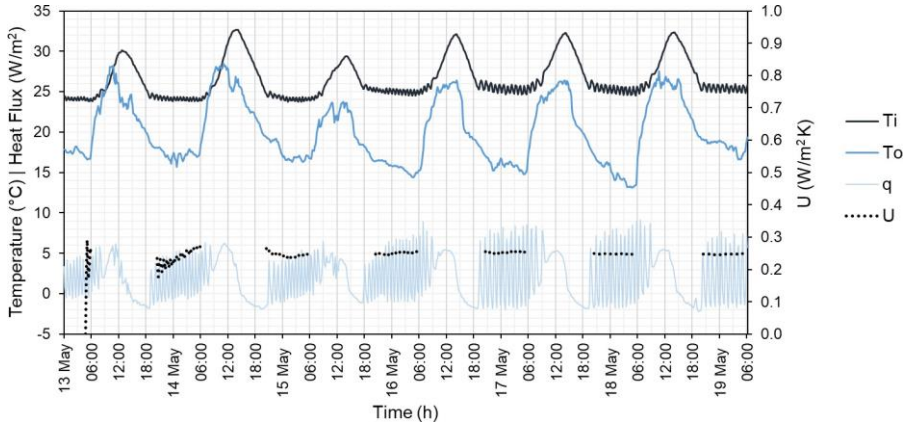

406 b

407 Fig. 6. a) Indoor and outdoor surface temperatures (*Tsi* and *Tso*, respectively), heat flux *q* and thermal conductance *Λ* obtained through
408 the average method; a) indoor and outdoor air temperatures (*Ti* and *To*, respectively), heat flux *q* and thermal transmittance *U* computed
409 through the average method. According to the average method in ISO 9869-1 [40], only the transmittance and conductance values
410 obtained at the end of the calculation (19 May, 6:00) can be considered as representative of the thermal behavior of the building
411 component.

412 3.2 Airtightness

413 The results of the blower door test obtained for each different configuration are reported in Table 6. All the test conditions
414 requirements were met during tests. Ambient parameters measured during the test and reported in Table 7 highlight the
415 correct environmental conditions, whereas the air flow exponent *n* is always slightly lower than the upper bound (1.0, see
416 Table 6). Concerning the latter, since theoretically *n* vary from 0.5 to 1.0 passing from a turbulent flow through large
417 openings to a laminar flow through small openings, then it can be said that most of the air leakage paths (ALP) of the unit
418 can be categorized as “small openings” [71,72].

419 Table 6. Airtightness test results.

Configuration	C_{env}	n	R^2	C_L	q_{50} (m^3/h)	n_{50} (h^{-1})	q_E (m^3/(h m^2))	q_F (m^3/(h m^2))
1 (Building in use and envelope)	4.294	0.737	0.993	4.264	76.05	2.55	1.21	6.11
2 (Sealed window)	2.587	0.714	0.980	2.568	41.95	1.40	0.67	3.37
3 (Sealed door)	0.691	0.990	0.981	0.686	32.98	1.10	0.52	2.65
4 (Sealed openings)	0.599	0.968	0.983	0.595	26.25	0.88	0.42	2.11

Table 7. Ambient parameters measured during the test for validation or data correction according to ISO 9972 [44]. T_i and T_o: indoor and outdoor air temperatures, respectively.

Configuration	T_i/T_o (°C)	Wind force (Beaufort scale)	Max wind speed (m/s)	Atm press (kPa)
1 (Building in use and envelope)	24.4/24.4	2	0.4 – 0.9	100.9
2 (Sealed window)	24.6/24.6	2	0.4 – 1.3	100.9
3 (Sealed door)	24.6/24.6	2	0.4 – 0.9	100.9
4 (Sealed openings)	24.2/24.2	2	0.9 – 1.3	100.9

The air change rates n_{50}, obtained for a pressure difference of 50 Pa, ranges from 0.88 h^{-1}, in case of configuration 4 with sealed openings, to 2.55 h^{-1} for configuration 1 without any additional sealing. This means that the joints between windows and doors were one of the most influencing factors affecting building airtightness. For this reason, a linear correlation between opening joint length and n_{50} is computed and plotted in Fig. 7. The correlation, with an R^2 value equal to 0.84, indicates that the joint between openings and panels has a strong influence on the airtightness of the construction system.

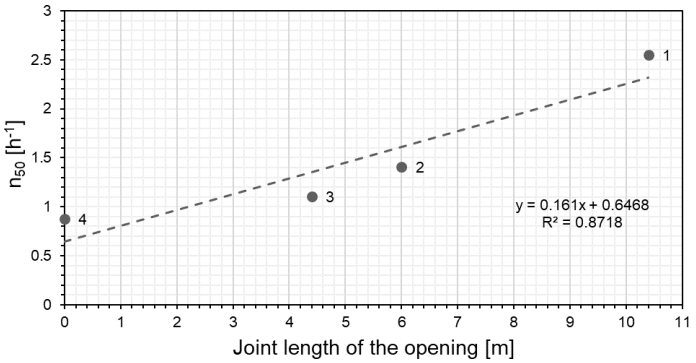

Fig. 7. Correlation between n_{50} values obtained for the different configurations and length of joints between openings and panels.

3.3 Hygrothermal behavior

In this paragraph, the results of the measurements carried out in order to investigate the indoor hygrothermal environment of the experimental unit are reported. In particular, due to the high amount of collected data, only representative results are shown in the following, i.e. the results of representative days with closed openings and clear sky, and of representative

days with a slightly open window and clear sky. It should be noted that, since same results were obtained for the different heat flux sensors and for the different surface temperature sensors placed on the inner side of the north wall, only the results of the central sensors are reported in this paragraph.

In Fig. 8, the measurement results of three representative days characterized by sunny weather, i.e. 8 March, 26 March and 11 April 2017, are reported. During these days, the window was closed in order to assemble the worst scenario that can occur in high-density emergency camps where, due to the presence of other housing units, the natural ventilation can be blocked [21]. These days were characterized by increasing outdoor air temperatures, ranging from 7°C to 13 °C on 8 March, from 10 to 18 °C on 11 April, and from 13 to 25 °C on 11 April. The peaks of global solar radiation were 715, 820 and 846 W/m^2, respectively, with an average share for the diffuse radiation at about 35% of the global radiation.

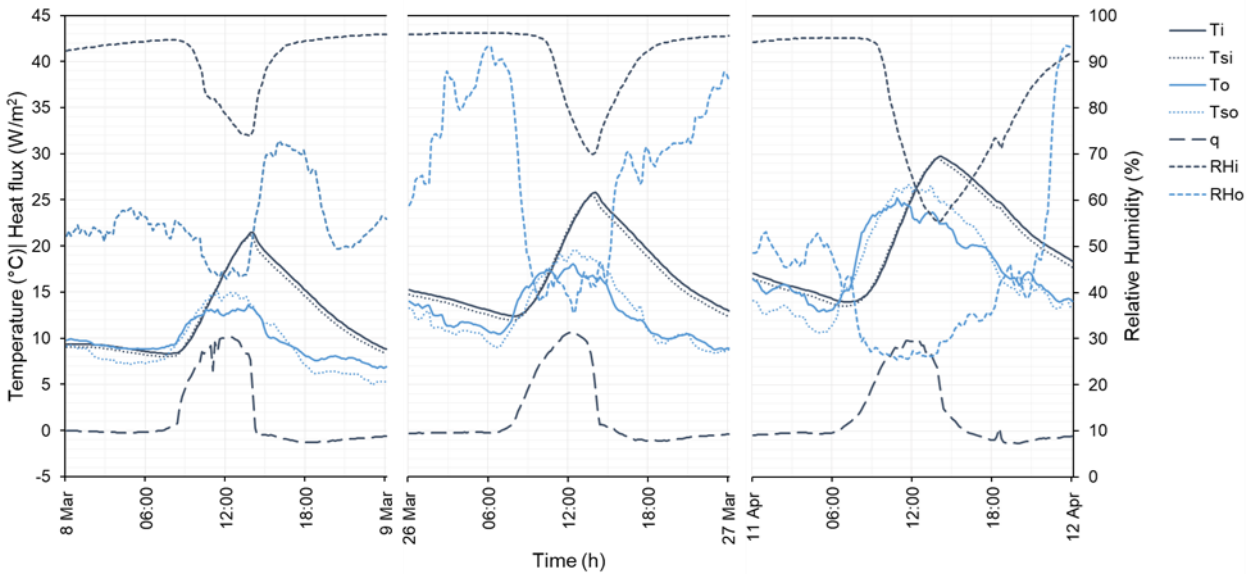

Fig. 8. Measurements results of three representative days with closed window and clear sky. *Ti*: indoor air temperature; *Tsi*: indoor surface temperature; *To*: outdoor air temperature; *Tso*: outdoor surface temperature; *q*: heat flux rate; *RHi*: indoor relative humidity; *RHo*: outdoor relative humidity.

First, a comparison between air and surface indoor temperatures, T_i and T_{si} respectively, is made. In particular, a very small temperature variation between T_i and T_{si} was found. This was probably due to the small size of the unit that did not allow a significant temperature variation inside the unit (Fig. 8).

Then, the behavior of the indoor environment during the days can be analyzed. In particular, all of the selected days can be subdivided in a heating period, from about 7:00 to about 14:00, and a cooling period, from 14:00 to 7:00 (Fig. 8). The heating period, in turn, can be subdivided into two main sub-phases. A first phase, in which the indoor temperature is lower than the outdoor one, and a second phase, where the indoor temperature is instead higher than the outdoor one.

In the first phase of the heating period, the effect of the high insulation properties of the construction system can be observed. In fact, from sunrise (i.e. at about 7:00) to 8:00 (i.e. when first solar beams previously obstructed by near buildings reached the window of the unit), the temperature of the outdoor environment T_o started to increase while T_i, generally lower than T_o, remained constant. This demonstrates the inability of the system to exchange heat through the envelope, as also shown by the very low heat flux rate q measured on the north wall during this phase (Fig. 8).

When the solar direct radiations, no more obstructed by near buildings, started penetrating inside the unit through the south window (from about 8:00), T_i started increasing. In the meanwhile, heat started to be transferred from outdoor to the indoor environment through the north wall, as also evidenced by the inward heat flux rate q measured on the north wall, which reached a maximum positive value of about 11 W/m^2 just at the end of this phase (Fig. 8).

In the second phase of the heating period, while T_o remained constant (or slightly decreases), T_i kept rising due to the solar heat gain that continued to reach the indoor environment through the south window, heating the indoor air up. In this phase, the maximum difference ΔT between T_i and T_o was reached, ranging between 6 and 9 °C. Clearly, the overheating of the indoor environment was accentuated by the fact that both window and door were closed, i.e. no heat loss due to natural ventilation was allowed. Since on average T_o remained constant in this phase, no significant thermal shift was noted between the indoor and outdoor air temperature peaks, highlighting, as expected, the quite null thermal storage of the system.

In this phase, and until 18:00, the outdoor surface temperatures of the north wall T_{so} were generally higher than T_o, with a maximum difference of about 3 °C. This was probably caused by the indirect solar radiation coming from the ground and near buildings that hit the external north surface.

During the cooling period, from about 14:00 to 7:00, due to the particular position of the unit with respect to other near constructions, the solar radiations did not penetrate anymore through the south window. As a result, T_i started decreasing, following the decrease of the solar heat gain. This notwithstanding, T_i remained constantly higher than T_o, denoting again the poor ability of the system to release the heat towards the external environment, as also evidenced by the very low negative (outward) heat flux q measured during this period in the north wall.

During the nighttime, i.e. from about 18:00 to about 7:00, the surface outdoor temperature T_{so} of the north wall was always lower than T_o, with a maximum temperature difference of 3 °C. This was probably due to the sky-cooling effect, i.e. the night heat loss of the envelope due to the longwave radiation heat exchange with the atmosphere [73–78].

Finally, concerning *RH*, with closed openings indoor air *RH* values were always higher than outdoor ones, with a quite constant value of about 95% during nighttime and a lower value during daytime due to the higher indoor air temperatures.

These high *RH* values were probably due to the daytime evaporation of the water drops formed during nighttime by condensation in the internal surface of the unit (observed in the morning mainly on the western panels junctions of the roof and on the panels junctions of the north wall, see Fig. 9), that adds humidity to the indoor environment until the maximum *RH* is reached. The cause of the condensation issues, probably a combined effect of sky cooling and thermal bridges, will be investigated through hygrothermal simulations in Section 3.4.

Fig. 9. Condensation observed during daytime.

In order to guarantee a higher moisture exchange between indoor and outdoor environment, simulating a more real use [21], the window was then slightly open with an opening area of 0.08 m^2. In Fig. 10, the measurement results of three representative days characterized by sunny weather and open window, i.e. 17 April and 18 and 24 June, are reported. During these days, the maximum T_o values ranged from 17°C to 37 °C. Peaks of global solar radiation were 909, 960 and 899 W/m^2, respectively, with an average share for the diffuse radiation at 40% of the global one.

As expected, due to the window opening, the indoor *RH* values were more similar to outdoor *RH* values, varying naturally in the range between 20% and 50%. Moreover, no water drops due to condensation caused by sky-cooling effects were noticed in this case. However, despite the higher natural ventilation for stack effect, from 12:00 to about 15:00 the solar radiations still caused the overheating of the indoor environment. In particular, a maximum ΔT between indoor and outdoor air temperature of about 7 °C was reached. Clearly, the overheating of the indoor environment, as well as the heat flux rate, was reduced by the fact that window was partially open, allowing a minimum, but not enough to prevent overheating, heat loss for natural ventilation.

Finally, some considerations about thermal comfort are reported by comparing the indoor operative temperature (assumed equal to the air temperature, see Section 2.6) with the acceptable operative temperature limits computed according to EN 15251 [47] (see Fig. 10). It should be noted that these are only preliminary considerations. Further and deeper analyses on this aspect will be carried out in future works.

As a general result, during nighttime, if the outdoor temperature is lower than the lower comfort limit, the indoor

thermal comfort is hardly reached despite the indoor temperature is generally higher than outdoor one (see e.g. 17th April and 18th June in Fig. 10). Then, occupants would feel cold especially during nighttime, suggesting to keep openings closed whenever possible in coldest hours unless the indoor temperature is lower than outdoor ones. Conversely, during the daytime, temperatures become more acceptable in the coldest days (i.e. 17th April in Fig. 10) while thermal discomfort easily occurs in the hottest ones for overheating of the indoor environment (see e.g. 18th and 24th April in Fig. 10). In this latter case, it is suggested to keep windows and doors open during the daytime, in order to maintain the indoor temperature similar to the outdoor one and to avoid overheating as much as possible.

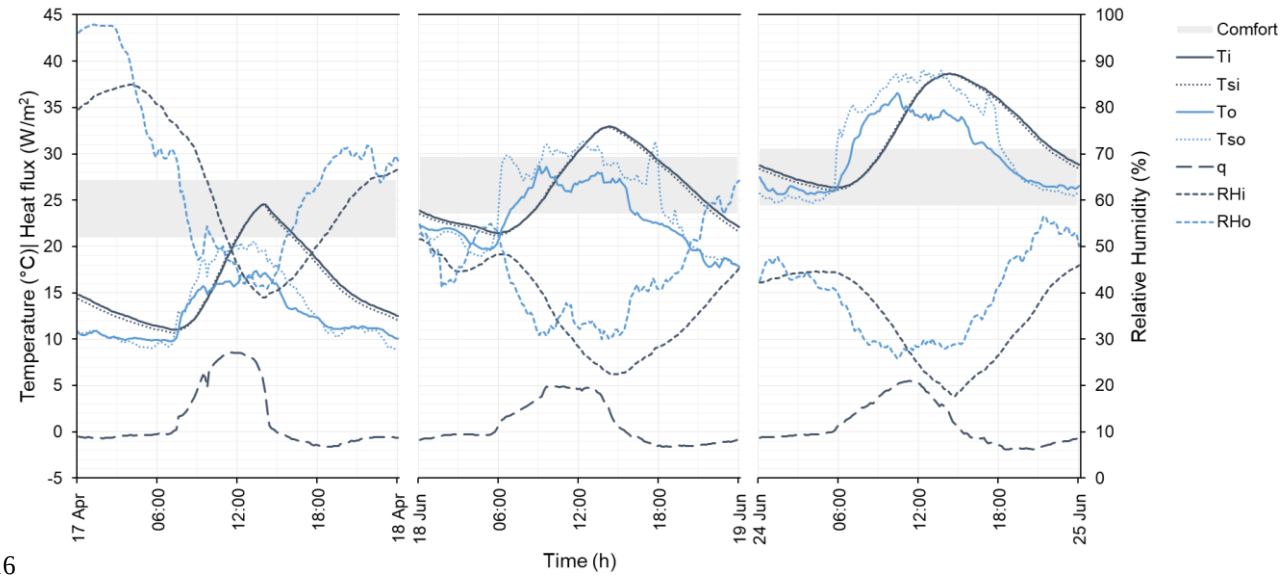

Fig. 10. Measurements results of three representative days with an open window and a clear sky. *Ti*: indoor air temperature; *Tsi*: indoor surface temperature; *To*: outdoor air temperature; *Tso*: outdoor surface temperature; *q*: heat flux rate; *RHi*: indoor relative humidity; *RHo*: outdoor relative humidity; Comfort: Comfort range computed according to EN 15251 [47].

3.4 Condensation risk and moisture safety

In Section 3.3, internal surface condensation issues at junctions were experimentally observed. For this reason, in this paragraph, the results of the hygrothermal dynamic simulations carried out to quantify the condensation and mold growth risk at the junctions during annual occupancy and in different climatic contexts are reported.

The impact of temperature on thermal conductivity was firstly evaluated by comparing the heat fluxes obtained by assuming a temperature-dependent λ with those obtained by assuming a constant λ. As already said in Section 2.7, a linear-dependent function was adopted in our work according to the experimental λ-T relationships obtained for EPS materials with different densities in [59,60] and to the in situ thermal conductivity obtained in Section 3.1 (λ=0.0288 W/mK for an average temperature at mid-thickness of 20.1°C). As a result, the following function was adopted to compute

λ during the hygrothermal simulation: $\lambda = 0.0276 + (6 \cdot 10^{-5}) \cdot T$ (in W/mK).

For all the considered climatic conditions, no significant differences were found between the two heat flux profiles (the root mean square error, RMSE, was always lower than 2% in all the seasons). Hence, assuming a constant value can be considered a good approximation in both hygrothermal and energy simulations.

Concerning condensation risk, Fig. 11 and Fig. 12 report the annual variations of the internal surface RH at roof and north wall junctions, respectively, while Fig. 13 reports the percentage of possible hours with condensation for both the heating and the cooling season (conventionally assumed in this work from October 1st to March 31th and from April 1st to September 30th, respectively). These graphs provide a first insight on the instants during the year and the hours of the days when the indoor surface RHs are excessively high.

The results obtained for the Ancona climate confirmed the experimental evidence. In fact, condensation occurred not only during the heating season but also in cooling season at nighttime, as experimentally observed in Section 3.3. For the roof panels, a higher number of hours with possible condensation were obtained if compared with those observed in the wall (Fig. 13). This difference can be mainly ascribable due to sky-cooling effect, which is generally more accentuated in the roof elements than in the wall ones [21]. Similar behavior was obtained for the other climates. In particular, the colder the climate, the higher the number of hours with condensation risk.

Finally, concerning moisture safety, Fig. 14 shows the mold index *M* obtained for the building component with higher condensation risk (i.e. the roof). Regardless of the climatic contexts, *M* quickly reaches a steady maximum value of about 3.5, mainly due to the quite continuous high RH values representing an optimal growth condition. This value represents a high and unacceptable risk of mold growth (see Table 4).

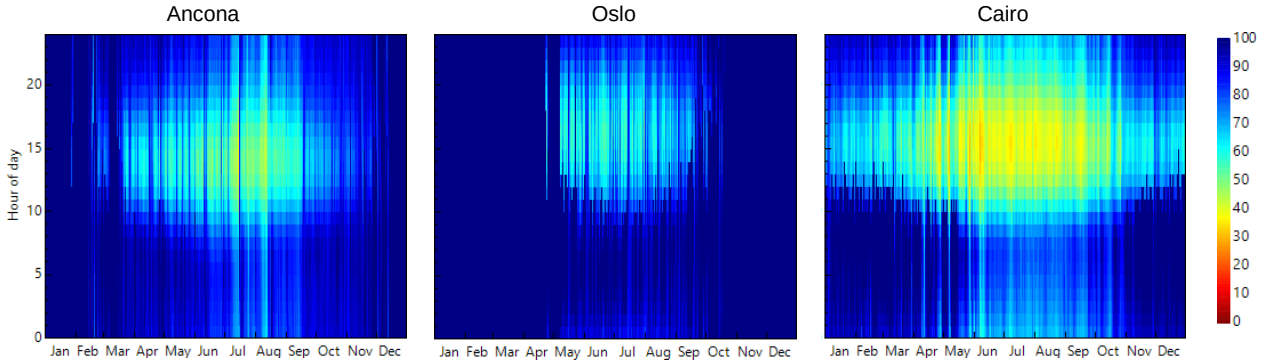

Fig. 11. Roof indoor surface RH at junction obtained through the numerical simulation for the three different climate scenarios.

Ancona Oslo Cairo

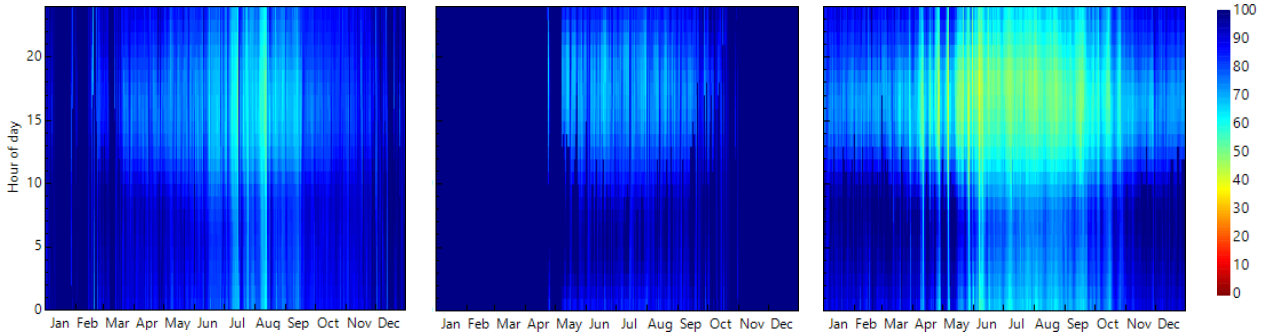

549 Fig. 12. North wall indoor surface RH at junction obtained through the numerical simulation for the three different climate scenarios.

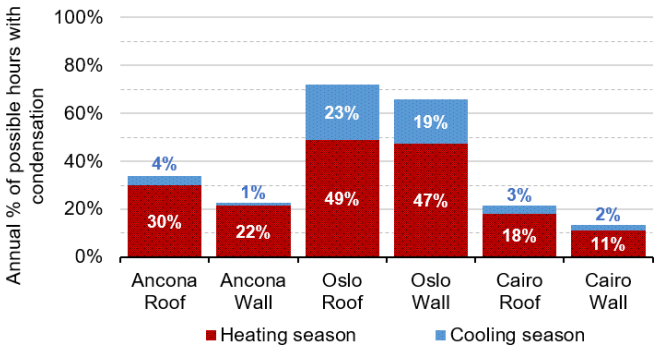

550

551 Fig. 13. Annual condensation risk for exterior roof and wall assemblies in different climatic scenarios for both the heating and the
552 cooling seasons.

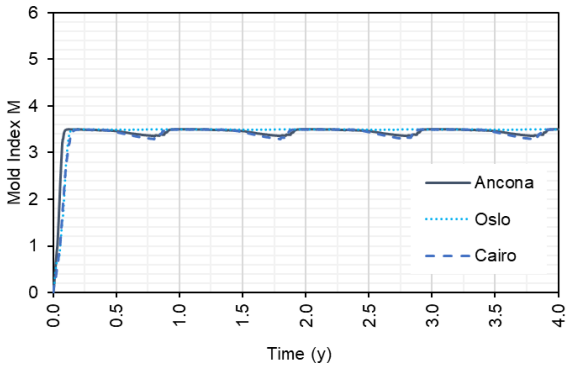

553

554 Fig. 14. Results from VTT damage model: mold index *M* on roof junctions.

555 3.5 Moisture buffering

556 Considering the results obtained in previous paragraphs (very high indoor RH and mold growth risk) a set of hygrothermal
557 simulations were carried out to verify the effectiveness of MB materials to improve the hygrometric behavior of the
558 system. In particular, the possible reduction of moisture-related issues achievable by adding two different types of internal
559 MB layers, i.e. a 3 mm thick cementitious rendering and a 12.5 mm thick gypsum plasterboard, was evaluated.

Fig. 15 reports for each climatic condition the computed indoor surface RH values at roof junctions, i.e. where the

higher condensation risk was recorded (see Section 3.4).

As a result, both the considered MB layers led to a significant reduction of surface RHs. In particular, for the basecoat case, the RH values are always lower than the condensation risk value (RH=95%), except for Oslo climate. In this latter case, the very cold winter temperatures led to a residual 6% of annual possible hours with condensation risk in both the heating and the cooling season. A higher moisture buffering capacity is needed in this case, that can be obtained, for example, by applying gypsum plasterboard (see Fig. 15).

Concerning the mold growth risk, the basecoat prevents mold growth in both Ancona and Cairo climates (see Fig. 16). Once again, however, gypsum plasterboard is needed in the Oslo climate to reach an M value equal to 0.

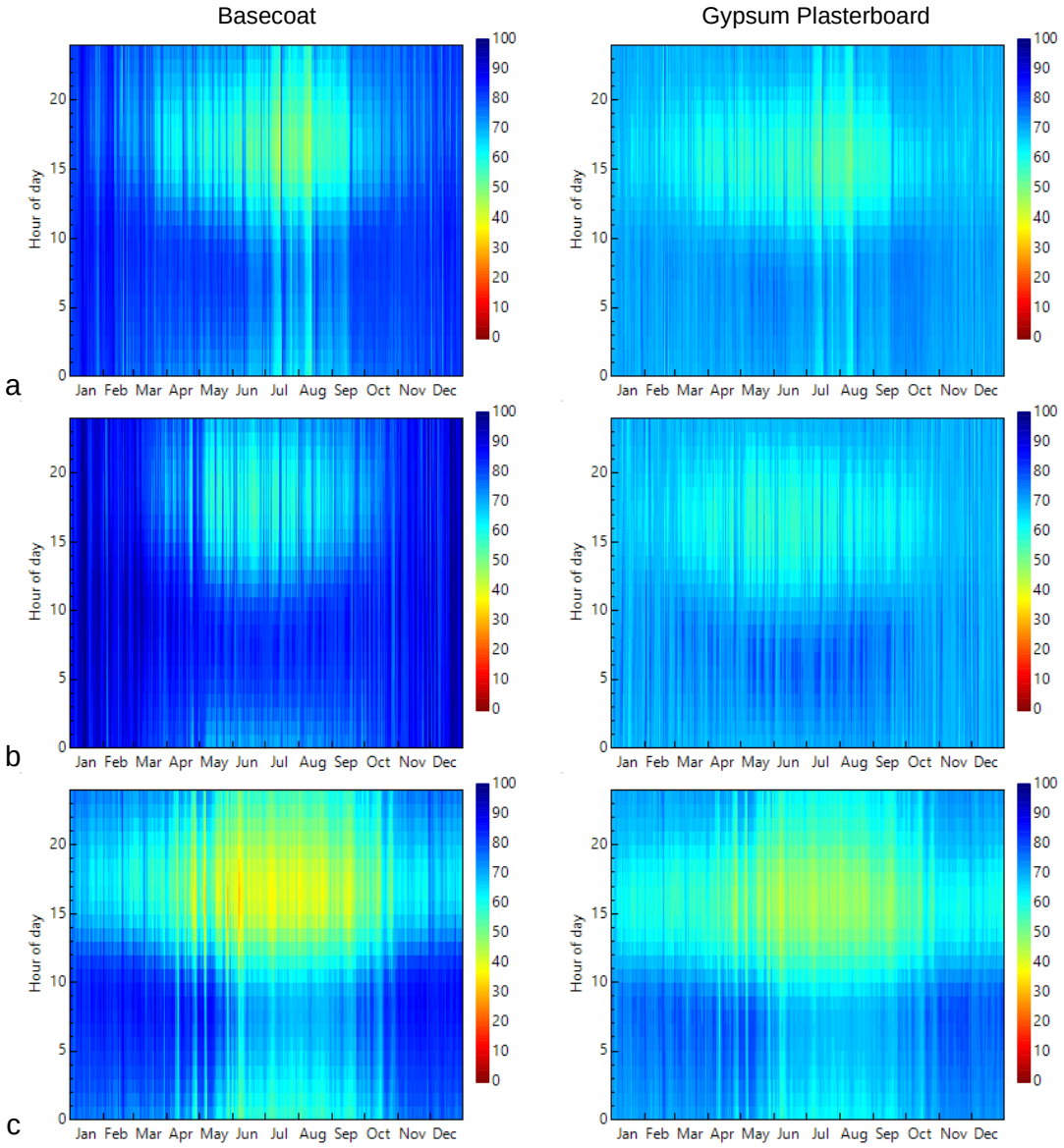

Fig. 15. Indoor surface RH at junction obtained through the numerical simulation in different climatic conditions: a) Ancona; b) Oslo; c) Cairo.

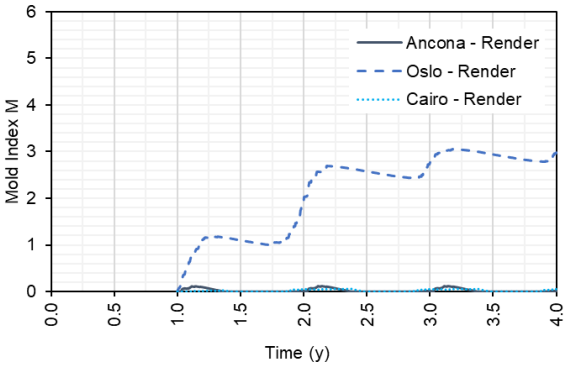

Fig. 16. Results from VTT damage model: mold index *M* at roof junction after applying a 3mm thick cementitious rendering layer on the inner side of the panels.

4 DISCUSSION

In this section, the main experimental results are discussed and commented. The experimental campaign allowed to characterize the HOMEDONE construction system and to investigate its indoor hygrothermal behavior.

The *in situ* experimental characterizations allowed to complete literature data, showing a low *in situ* thermal transmittance of the HOMEDONE panels and a good airtightness performance of the assembled unit. In particular, a U-value equal to 0.24 W/m^2 K was obtained. This value is lower than those characterizing common temporary houses (ranging from 0.43 to 0.60 W/m2 K, see [27]) and even lower than those prescribed by the Italian regulations for walls, slabs and roofs of new buildings located in Ancona, Italy (i.e. where the unit is located and equal to 0.34, 0.32 and 0.30 W/m2 K, respectively) [79]. This is due to the high thickness of the EPS panels, whose thermal insulation capacity were not affected by the presence of the embedded steel wire mesh. If a good airtightness is ensured, this result clearly implicates a better thermal and energy performance in the heating season of the HOMEDONE system in comparison with common container houses.

Concerning the airtightness, an *n50* equal to 2.55 h^{-1} was obtained for the studied unit. In this case, a comparison in general terms with other construction systems cannot be made due to the different factors that generally affect *n50* values and that may vary from one case to another (such as, for example, the geometry of the unit, the number and the type of the openings, finishing system etc.). However, for the specific case, the obtained *n50* value (2.55 h^{-1}) is lower than that obtained in literature for other types of temporary units (i.e. for common container houses *n50* ranges from 9.0 to 25.0 h-1, see [27]). This is probably due to the good sealing of the panels (obtained by means of silicone sealant), to the absence of building components related to electrical, architectural, water and air systems, but also to the presence of few openings.

In fact, it was seen that the opening contribution to air leakage for the studied unit is about 65%, which is higher than the contribution of common openings in standard construction systems (ranging from 4% to 50% with an average of 15% in Sothern Europe buildings, see [80]). An improvement of the airtightness performance of the system could be obtained, on one hand, by improving the quality of opening/panel junction detailing, and on the other hand by applying internal and external finishing systems on the unit (in this work no finishing systems were applied in order to simulate the worst scenario in terms of possible use).

Concerning the indoor hygrothermal measurements, the experimental campaign allowed to investigate the hygrothermal response of the experimental unit when subject to external ambient factors. In particular, the measurements revealed that, in absence of HVAC, solar shading devices and natural ventilation (as may occur in high-density emergency camp), the indoor air temperatures of the experimental unit considerably exceed outdoor ones (for a maximum of about 7°C during daytime) with a quite null thermal shift. This behavior is similar to that observed for other types of lightweight temporary disaster-relief houses (see e.g. [21], [26] and [25]) and can be mainly attributable to the insufficient internal thermal storage capacity of the EPS material, the low thermal transmittance of the HOMEDONE panels and the good airtightness of the system. In fact, differently from common heavyweight construction systems, in which building components have higher internal thermal inertia [81], the insufficient thermal storage capacity of the panels did not allow the dampening of the indoor air temperatures, also resulting in a thermal response quite synchronized with external ambient factors (in this case mainly the solar radiation passing through the window). Moreover, the slow outwards heat transfer, caused by the low *in situ* thermal transmittances and the good airtightness of the system, fosters the overheating of the indoor environment during the daytime.

Concerning RH levels, in case of closed window, indoor RH values reach a constant value of 95% during nighttime, mainly due to the low capacity of the EPS to absorb water in the internal side of the panels [63]. During the nighttime, in fact, the internal surface temperatures of junctions become lower than the indoor air temperature, as verified through numerical hygrothermal simulations. As a result, several water drops are generated by condensation on the internal surfaces. Then, due to the inability of the EPS panels to absorb liquid water on their inner side, water drops evaporate during the day, constantly adding moisture to the indoor environment until high RH values are reached. The limited vapor permeability of the EPS, along with the quite null natural ventilation due to the good airtightness performance, prevents the vapor transmission between indoor and outdoor environment, keeping the indoor moisture levels constantly higher than outdoor ones. This constitutes an unhealthy condition for the occupants, due to the related mold growth risk [52].

However, it was experimentally demonstrated that if a minimum of natural ventilation is ensured (by slightly opening

623 the window, as may occur in real condition of use, or by considering the lower airtightness of the unit that may result in
624 case of a higher number of opening), the indoor humidity levels quickly approach outdoor ones. Besides, the hygrothermal
625 simulations showed that an internal finishing layer with an adequate moisture buffering capacity, such as 3mm thick
626 cementitious basecoat in hot climates or a 12.5cm thick gypsum plasterboard in cold climates, can prevent surface
627 condensation and mold growth.

628 Finally, based on the preliminary comfort evaluations carried out in this study, some general and conclusive
629 considerations can be drawn, as reported in the following.

630 In the heating season, the overheating of the indoor environment may have a beneficial impact on occupants' comfort.
631 However, in cloudy/rainy days, the overheating of the indoor environment due to solar heat gain is hardly obtained. At
632 nighttime, moreover, indoor temperatures approach outdoor ones due to the low thermal storage capacity of the system.
633 Thence, the construction system cannot ensure complete protection from winter environment if a heating apparatus is not
634 introduced.

635 In the cooling season, during the daytime, the overheating of the indoor environment may have a negative impact on
636 occupants' comfort. Air temperature, in fact, could exceed the skin temperature of occupants causing an uncomfortable
637 condition for the human body, that cannot dissipate heat by radiation or convection, but by sweating only. In this case,
638 due to the absence of an HVAC system, passive cooling measures could be applied in order to improve the thermal
639 comfort inside the unit, such as, for example, shading device, increasing the internal thermal storage capacity or enhancing
640 natural ventilation.

641 At nighttime, conversely, the low thermal transmittance of the unit and the good airtightness keep the indoor
642 temperatures higher than outdoor ones, making the indoor conditions more acceptable for occupants. However, if
643 adequate ventilation is not ensured, RH values may reach very high and uncomfortable values due to the presence of
644 thermal bridge at the junctions and the null absorbing capacity of the EPS material. These factors, together, lead to the
645 generation of water drops that evaporate during daytime (since not absorbed by the panels), increasing air moisture level.
646 It should be noted that, in the presence of occupants, additional heat and moisture is added to the indoor environment,
647 increasing the potential for condensation.

648 As a result, due to the simultaneous presence of unacceptable temperatures and moisture level in the cooling season,
649 occupants can easily suffer from heatstroke, while unhealthy indoor conditions due to mold growth may occur. Then, the
650 studied construction system should be not used on a long-term basis if appropriate measures to improve the thermal
651 environment inside the unit, such as applying passive cooling techniques and increasing the panel moisture buffering

652 capacity, are not previously adopted.

653 5 CONCLUSIONS

654 In this paper, an experimental and numerical study on the indoor hygrothermal behavior of a novel post-disaster temporary
655 housing solution, named HOMEDONE, based on the assembly of reinforced-EPS panels, was presented.

656 Firstly, in order to complete the available literature data, a characterization of the system was carried out by measuring
657 the *in situ* thermal transmittance and airtightness performance of an experimental unit. Then, an experimental campaign
658 was carried out in order to fully understand its indoor hygrothermal behavior and to identify any possible internal
659 condensation issues. Finally, several hygrothermal simulations were performed for investigating the occurrence of the
660 experimentally observed condensation issues during annual occupancy and under different climatic contexts, for
661 quantifying the related mold growth risk and, finally, for evaluating the possible reduction of these issues by adding
662 interior moisture buffering materials.

663 The results revealed that the studied construction system has good thermal transmittance (U-value equal to 0.24 W/m^2
664 K) and airtightness performance (*n50* equal to 2.55 h^{-1}). Concerning the latter, it is also found that a significant
665 improvement of airtightness performance could be obtained by improving the quality of opening/panel junction detailing.
666 The measured indoor hygrothermal environment, instead, revealed that, at closed opening conditions, the indoor air
667 temperature can be very high and unacceptable in hot seasons. Moreover, if a minimum of air ventilation is not guaranteed,
668 even the relative humidity results highly unacceptable, especially during nighttime. This was mainly due to the quite null
669 internal thermal storage capacity and the null moisture buffering capacity of the HOMEDONE panels. In particular, the
670 null moisture buffering capacity does not allow the absorption of the water drops generated during nighttime from internal
671 surface condensation at junctions, that, in turn, evaporates during daytime increasing the moisture level. Conversely, if a
672 minimum of ventilation is guaranteed, relative humidity quickly approaches the outdoor one.

673 Finally, the hygrothermal simulations showed that an internal finishing layer with an adequate moisture buffering
674 capacity, such as 3mm thick cementitious basecoat in hot climates or a 12.5cm thick gypsum plasterboard in cold climates,
675 can prevent internal surface condensation and mold growth.

676 In conclusion, an unacceptable indoor hygrothermal environment can occur during cooling season inside the
677 HOMEDONE temporary housing solutions, which can be detrimental for occupants' health. Thus, since these temporary
678 lightweight houses are increasingly used for long periods of occupancy rather than for the short periods, appropriate
679 measures should be adopted to improve their indoor thermal environment and comfort, allowing a safer long-term use.
680 With this aim, further experimental and numerical studies are being carried out to evaluate how passive cooling measures

681 can improve the thermal environment of this construction system and to make it more thermally comfortable and safe for
682 the occupants.

683 6 ACKNOWLEDGMENTS

684 Financial support for this study was provided by the AC-Engineering S.p.A under the “POR FESR Marche 2014/2020”
685 Research Project No. 15345.

686 7 REFERENCES

687 [1] Eurostat, Migration and migrant population statistics - Statistics Explained, (2018).
688 http://ec.europa.eu/eurostat/statistics-explained/index.php/Migration_and_migrant_population_statistics
689 (accessed December 27, 2017).
690 [2] Centre for Research on the Epidemiology of Disasters (CRED), The international disasters database, (2017).
691 http://www.emdat.be/ (accessed December 27, 2017).
692 [3] D. Félix, D. Monteiro, J.M. Branco, R. Bologna, A. Feio, The role of temporary accommodation buildings for
693 post-disaster housing reconstruction, J. Hous. Built Environ. 30 (2014) 683–699. doi:10.1007/s10901-014-9431-
694 4.
695 [4] D. Félix, J.M. Branco, A. Feio, Temporary housing after disasters: A state of the art survey, Habitat Int. 40 (2013)
696 136–141. doi:10.1016/j.habitatint.2013.03.006.
697 [5] International Federation of Red Cross and Red Crescent Societies (IFRC), Post-disaster shelter: Ten designs,
698 (2013). www.ifrc.org.
699 [6] M. Arouri, C. Nguyen, A. Ben Youssef, Natural Disasters, Household Welfare, and Resilience: Evidence from
700 Rural Vietnam, World Dev. (2015). doi:10.1016/j.worlddev.2014.12.017.
701 [7] Y.A. Chang-Richards, S. Wilkinson, E. Seville, D. Brunsdon, Provision of temporary accommodation for
702 construction workers Learnings from Queensland post Cyclone Larry, (2014). https://resorgs.org.nz/wp-
703 content/uploads/2017/07/provision_of_workers_accommodation.pdf (accessed December 22, 2017).
704 [8] A. Salehi, I. Torres, A. Ramos, Experimental analysis of building airtightness in traditional residential Portuguese
705 buildings, Energy Build. 151 (2017) 198–205. doi:10.1016/j.enbuild.2017.06.037.
706 [9] Y. Ji, L. Duanmu, X. Li, Building air leakage analysis for individual apartments in North China, Build. Environ.
707 122 (2017) 105–115. doi:10.1016/j.buildenv.2017.06.007.
708 [10] S. Shi, C. Chen, B. Zhao, Air infiltration rate distributions of residences in Beijing, Build. Environ. 92 (2015)

528–537. doi:10.1016/j.buildenv.2015.05.027.

[11] J. Jokisalo, J. Kurnitski, M. Korpi, T. Kalamees, J. Vinha, Building leakage, infiltration, and energy performance analyses for Finnish detached houses, Build. Environ. 44 (2009) 377–387. doi:10.1016/j.buildenv.2008.03.014.

[12] M. Steeman, A. Janssens, H.J. Steeman, M. Van Belleghem, M. De Paepe, On coupling 1D non-isothermal heat and mass transfer in porous materials with a multizone building energy simulation model, Build. Environ. 45 (2010) 865–877. doi:10.1016/j.buildenv.2009.09.006.

[13] T. Kalamees, Air tightness and air leakages of new lightweight single-family detached houses in Estonia, Build. Environ. 42 (2007) 2369–2377. doi:10.1016/j.buildenv.2006.06.001.

[14] UNRWA - United Nations Relief and Works Agency for Palestine refugees in the near east, Palestine refugees | UNRWA, (n.d.). https://www.unrwa.org/palestine-refugees (accessed September 19, 2018).

[15] UNHCR - The UN Refugee Agency, UNHCR - Figures at a Glance. Statistical yearbooks, (2019). http://www.unhcr.org/uk/figures-at-a-glance.html (accessed September 19, 2018).

[16] IDMC, Global Internal Displacement Database | IDMC, (2018). http://www.internal-displacement.org/database (accessed September 19, 2018).

[17] IDMC, GRID 2018 | Global Report on Internal Displacement 2018, (2018). http://internal-displacement.org/global-report/grid2018/ (accessed September 19, 2018).

[18] M. Lee, L. Shi, A. Zanobetti, J.D. Schwartz, Study on the association between ambient temperature and mortality using spatially resolved exposure data, Environ. Res. (2016). doi:10.1016/j.envres.2016.08.029.

[19] D. Albadra, M. Vellei, D. Coley, J. Hart, Thermal comfort in desert refugee camps: An interdisciplinary approach, Build. Environ. 124 (2017) 460–477. doi:10.1016/j.buildenv.2017.08.016.

[20] N. Shinohara, M. Tokumura, K. Hashimoto, K. Asano, Y. Kawakami, Fungal levels in houses in the Fukushima Daiichi nuclear power plant evacuation zone after the great east Japan earthquake, J. Air Waste Manag. Assoc. 67 (2017) 1106–1114. doi:10.1080/10962247.2017.1330712.

[21] Y. Wang, L. Wang, E. Long, S. Deng, An experimental study on the indoor thermal environment in prefabricated houses in the subtropics, Energy Build. 127 (2016) 529–539. doi:10.1016/j.enbuild.2016.05.061.

[22] R. Thapa, H.B. Rijal, M. Shukuya, Field study on acceptable indoor temperature in temporary shelters built in Nepal after massive earthquake 2015, Build. Environ. 135 (2018) 330–343.doi:10.1016/j.buildenv.2018.03.001.

[23] F. Barreca, V. Tirella, A self-built shelter in wood and agglomerated cork panels for temporary use in Mediterranean climate areas, Energy Build. 142 (2017) 1–7. doi:10.1016/j.enbuild.2017.03.003.

738 [24] J.-G. Kim, J. Lee, B.-L. Ahn, H. Shin, S. Yoo, C.-Y. Jang, D. Song, J. Kim, Indoor Thermal Environment of
739 Temporary Mobile Energy Shelter Houses (MeSHs) in South Korea, Energies. 8 (2015) 11139–11152.
740 doi:10.3390/en81011139.
741 [25] D. Albadra, D. Coley, J. Hart, Toward healthy housing for the displaced, J. Archit. 23 (2018) 115–136.
742 doi:10.1080/13602365.2018.1424227.
743 [26] L. Huang, E. Long, J. Ouyang, Measurement of the Thermal Environment in Temporary Settlements with High
744 Building Density after 2008 Wenchuan Earthquake in China, Procedia Eng. 121 (2015) 95–100.
745 doi:10.1016/j.proeng.2015.08.1027.
746 [27] A.M. Tanyer, A. Tavukcuoglu, M. Bekboliev, Assessing the airtightness performance of container houses in
747 relation to its effect on energy efficiency, Build. Environ. 134 (2018) 59–73. doi:10.1016/j.buildenv.2018.02.026.
748 [28] H. Wallbaum, Y. Ostermeyer, C. Salzer, E. Zea Escamilla, Indicator based sustainability assessment tool for
749 affordable housing construction technologies, Ecol. Indic. 18 (2012) 353–364.
750 doi:10.1016/j.ecolind.2011.12.005.
751 [29] N.H. Ramli Sulong, S.A.S. Mustapa, M.K. Abdul Rashid, Application of expanded polystyrene (EPS) in buildings
752 and constructions: A review, J. Appl. Polym. Sci. (2019) 47529. doi:10.1002/app.47529.
753 [30] A.S. Sferra, Emergency: innovative prefabricated construction components for an eco-solidarity architecture,
754 TECHNE - J. Technol. Archit. Environ. (2017) 328–334. doi:10.13128/Techne-20788.
755 [31] (CEN) European Committee for Standardisation, EN 10027-1: 2005 Designation systems for steels - Part 1: Steel
756 names, Eur. Stand. 3 (2005) 1–25.
757 [32] E. Wagemann, Need for adaptation: transformation of temporary houses, Disasters. 41 (2017) 828–851.
758 doi:10.1111/disa.12228.
759 [33] H. Arslan, Re-design, re-use and recycle of temporary houses, Build. Environ. 42 (2007) 400–406.
760 doi:10.1016/j.buildenv.2005.07.032.
761 [34] M. Kottek, J. Grieser, C. Beck, B. Rudolf, F. Rubel, World map of the Köppen-Geiger climate classification
762 updated, Meteorol. Zeitschrift. (2006). doi:10.1127/0941-2948/2006/0130.
763 [35] G. Desogus, S. Mura, R. Ricciu, Comparing different approaches to in situ measurement of building components
764 thermal resistance, Energy Build. 43 (2011) 2613–2620. doi:10.1016/j.enbuild.2011.05.025.
765 [36] G. Ficco, F. Iannetta, E. Ianniello, F. Romana, M. Dell, U -value in situ measurement for energy diagnosis of
766 existing buildings, Energy Build. 104 (2015) 108–121. doi:10.1016/j.enbuild.2015.06.071.

[37] P. Baker, U - values and traditional buildings, Hist. Scotl. Tech. Pap. 10. (2011) 70. http://www.historic-scotland.gov.uk/hstp102011-u-values-and-traditional-buildings.pdf.

[38] F. Asdrubali, F. D'Alessandro, G. Baldinelli, F. Bianchi, Evaluating in situ thermal transmittance of green buildings masonries: A case study, Case Stud. Constr. Mater. 1 (2014) 53–59. doi:10.1016/j.cscm.2014.04.004.

[39] L. Evangelisti, C. Guattari, P. Gori, R. De Lieto Vollaro, In situ thermal transmittance measurements for investigating differences between wall models and actual building performance, Sustain. 7 (2015) 10388–10398. doi:10.3390/su70810388.

[40] ISO 9869-1, Thermal insulation -- Building elements -- In-situ measurement of thermal resistance and thermal transmittance Heat flow meter method, 2014.

[41] A. Deconinck, S. Roels, Comparison of characterisation methods determining the thermal resistance of building components from onsite measurements, Energy Build. 130 (2016) 309–320. doi:10.1016/j.enbuild.2016.08.061.

[42] I.A. Atsonios, I.D. Mandilaras, D.A. Kontogeorgos, M.A. Founti, A comparative assessment of the standardized methods for the in–situ measurement of the thermal resistance of building walls, Energy Build. 154 (2017) 198–206. doi:10.1016/j.enbuild.2017.08.064.

[43] ASTM C1155-95. Standard Practice for Determining Thermal Resistance of Building Envelope Components from the In-situ Data, 2007.

[44] EN ISO 9972:2015. Thermal performance of buildings - Determination of air permeability of buildings - Fan pressurization method, (2015).

[45] Y. Ji, L. Duanmu, Airtightness field tests of residential buildings in Dalian, China, Build. Environ. 119 (2017) 20–30. doi:10.1016/j.buildenv.2017.03.043.

[46] ASHRAE, ASHRAE Handbook-Fundamentals, ASHRAE Handbook-Fundamentals. (2013) 21.1-21.67. doi:10.1017/CBO9781107415324.004.

[47] EN 15251, Indoor environmental input parameters for design and assessment of energy performance of buildings-addressing indoor air quality, thermal environment, lighting and acoustics, (2007).

[48] M. Marocco, F. Orlandi, Qualità del comfort ambientale. Elementi per la progettazione, Editrice Dedalo Roma, Roma, Italy, 2000.

[49] P. Samani, V. Leal, A. Mendes, N. Correia, Comparison of passive cooling techniques in improving thermal comfort of occupants of a pre-fabricated building, Energy Build. 120 (2016) 30–44. doi:10.1016/j.enbuild.2016.03.055.

[50] N. Walikewitz, B. Jänicke, M. Langner, F. Meier, W. Endlicher, The difference between the mean radiant temperature and the air temperature within indoor environments: A case study during summer conditions, Build. Environ. 84 (2015) 151–161. doi:10.1016/j.buildenv.2014.11.004.

[51] E. Vereecken, S. Roels, Review of mould prediction models and their influence on mould risk evaluation, Build. Environ. 51 (2012) 296–310. doi:10.1016/j.buildenv.2011.11.003.

[52] E. Di Giuseppe, Nearly Zero Energy Buildings and Proliferation of Microorganisms, Springer International Publishing, Cham, 2013. doi:10.1007/978-3-319-02356-4.

[53] J. Grunewald, Diffusiver und konvektiver Stoff-und Energietransport, University of Technology Dresden, Germany, 1997.

[54] J.M.P.Q. Delgado, N.M.M. Ramos, E. Barreira, V.P. de Freitas, A CRITICAL REVIEW OF HYGROTHERMAL MODELS USED IN POROUS BUILDING MATERIALS, J. Porous Media. 13 (2010) 221–234. doi:10.1615/JPorMedia.v13.i3.30.

[55] S. Claude, S. Ginestet, M. Bonhomme, G. Escadeillas, J. Taylor, V. Marincioni, I. Korolija, H. Altamirano, Evaluating retrofit options in a historical city center: Relevance of bio-based insulation and the need to consider complex urban form in decision-making, Energy Build. 182 (2019) 196–204. doi:10.1016/j.enbuild.2018.10.026.

[56] P. Pihelo, T. Kalamees, The effect of thermal transmittance of building envelope and material selection of wind barrier on moisture safety of timber frame exterior wall, J. Build. Eng. 6 (2016) 29–38. doi:10.1016/j.jobe.2016.02.002.

[57] U. Berardi, The impact of aging and environmental conditions on the effective thermal conductivity of several foam materials, Energy. 182 (2019) 777–794. doi:10.1016/j.energy.2019.06.022.

[58] U. Berardi, M. Naldi, The impact of the temperature dependent thermal conductivity of insulating materials on the effective building envelope performance, Energy Build. 144 (2017) 262–275. doi:10.1016/j.enbuild.2017.03.052.

[59] M. Khoukhi, N. Fezzioui, B. Draoui, L. Salah, The impact of changes in thermal conductivity of polystyrene insulation material under different operating temperatures on the heat transfer through the building envelope, Appl. Therm. Eng. 105 (2016) 669–674. doi:10.1016/j.applthermaleng.2016.03.065.

[60] M. Khoukhi, The combined effect of heat and moisture transfer dependent thermal conductivity of polystyrene insulation material: Impact on building energy performance, Energy Build. 169 (2018) 228–235. doi:10.1016/j.enbuild.2018.03.055.

825 [61] Á. Lakatos, Moisture induced changes in the building physics parameters of insulation materials, Sci. Technol.
826 Built Environ. 22 (2016) 252–260. doi:10.1080/23744731.2016.1131567.
827 [62] S. Cai, B. Zhang, L. Cremaschi, Review of moisture behavior and thermal performance of polystyrene insulation
828 in building applications, Build. Environ. 123 (2017) 50–65. doi:10.1016/j.buildenv.2017.06.034.
829 [63] Á. Lakatos, F. Kalmár, Analysis of water sorption and thermal conductivity of expanded polystyrene insulation
830 materials, Build. Serv. Eng. Res. Technol. 34 (2013) 407–416. doi:10.1177/0143624412462043.
831 [64] S. Schiavoni, F. D'Alessandro, F. Bianchi, F. Asdrubali, Insulation materials for the building sector: A review
832 and comparative analysis, Renew. Sustain. Energy Rev. 62 (2016) 988–1011. doi:10.1016/j.rser.2016.05.045.
833 [65] U.S. Department of Energy, Input Output Reference: The Encyclopedic Reference to EnergyPlus Input and
834 Output, 2012.
835 [66] EN 15026, Hygrothermal performance of building components and building elements - Assessment of moisture
836 transfer by numerical simulation, CEN. (2007).
837 [67] T. Ojanen, H. Viitanen, R. Peuhkuri, K. Lähdesmäki, J. Vinha, K. Salminen, Mold Growth Modeling of Building
838 Structures Using Sensitivity Classes of Materials, Therm. Perform. Exter. Envel. Build. XI. (2010).
839 [68] H. Viitanen, M. Krus, T. Ojanen, V. Eitner, D. Zirkelbach, Mold risk classification based on comparative
840 evaluation of two established growth models, Energy Procedia. 78 (2015) 1425–1430.
841 doi:10.1016/j.egypro.2015.11.165.
842 [69] EN 13163:2009. Thermal insulation products for buildings - Factory made expanded polystyrene (EPS) products
843 - Specification, (2009).
844 [70] EN ISO 6946:2007. Building components and building elements. Thermal resistance and thermal transmittance.
845 Calculation method, 2007.
846 [71] M.W. Liddament, Air Infiltration Calculation Techniques - an Application Guide, Air Infiltration and Ventilation
847 Center, Coventry, 1986.
848 [72] ATTMA, Measuring Air Permeability of Building Envelopes (Dwellings): Technical Standard 1, The Air
849 Tightness Testing and Measurement Association (ATTMA), Northampton, UK, 2010.
850 [73] S. Johansson, L. Wadsö, K. Sandin, Estimation of mould growth levels on rendered façades based on surface
851 relative humidity and surface temperature measurements, Build. Environ. 45 (2010) 1153–1160.
852 doi:10.1016/j.buildenv.2009.10.022.
853 [74] Y. Wang, E. Long, S. Deng, Applying passive cooling measures to a temporary disaster-relief prefabricated house

to improve its indoor thermal environment in summer in the subtropics, Energy Build. 139 (2017) 456–464. doi:10.1016/j.enbuild.2016.12.081.

[75] D. Aelenei, F.M.A. Henriques, Analysis of the condensation risk on exterior surface of building envelopes, Energy Build. 40 (2008) 1866–1871. doi:10.1016/j.enbuild.2008.04.003.

[76] K. Pietrzyk, A systemic approach to moisture problems in buildings for mould safety modelling, Build. Environ. 86 (2015) 50–60. doi:10.1016/j.buildenv.2014.12.013.

[77] G. Reynders, J. Diriken, D. Saelens, Generic characterization method for energy flexibility: Applied to structural thermal storage in residential buildings, Appl. Energy. 198 (2017) 192–202. doi:10.1016/j.apenergy.2017.04.061.

[78] E. Barreira, J.M.P.Q. Delgado, N.M.M. Ramos, V.P. de Freitas, Exterior condensations on façades: Numerical simulation of the undercooling phenomenon, J. Build. Perform. Simul. 6 (2013) 337–345. doi:10.1080/19401493.2011.560685.

[79] DM 26/06/2015 - "Requisiti minimi" Schemi e modalità di riferimento per la compilazione della relazione tecnica di progetto ai fini dell'applicazione delle prescrizioni e dei requisiti minimi di prestazione energetica negli edifici (in Italian), 2015.

[80] R.M.S.F. Almeida, N.M.M. Ramos, P.F. Pereira, A contribution for the quantification of the influence of windows on the airtightness of Southern European buildings, Energy Build. 139 (2017) 174–185. doi:10.1016/j.enbuild.2017.01.012.

[81] C. Di Perna, F. Stazi, A.U. Casalena, M. D'Orazio, Influence of the internal inertia of the building envelope on summertime comfort in buildings with high internal heat loads, Energy Build. 43 (2011) 200–206. doi:10.1016/j.enbuild.2010.09.007.